JCI The Journal of Clinical Investigation

Single cell transcriptomic analysis of renal allograft rejection reveals insights into intragraft TCR clonality

Tiffany Shi, … , E. Steve Woodle, David A. Hildeman

J Clin Invest. 2023. https://doi.org/10.1172/JCI170191.

Research In-Press Preview **Immunology** **Transplantation**

Graphical abstract

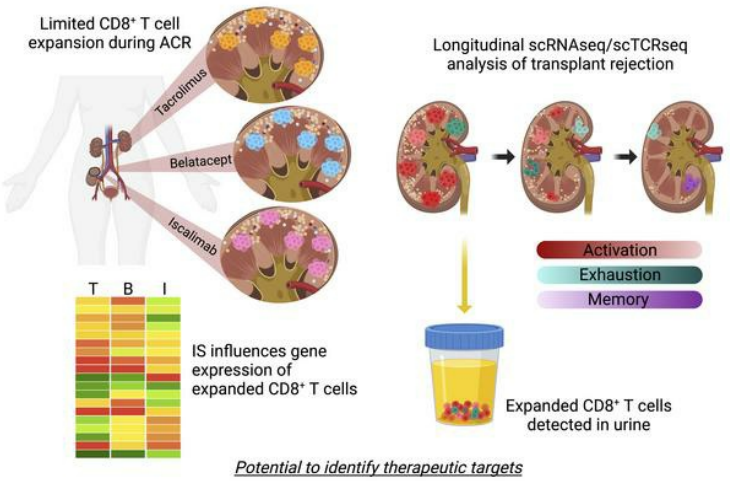

Find the latest version:

https://jci.me/170191/pdf

SINGLE CELL TRANSCRIPTOMIC ANALYSIS OF RENAL ALLOGRAFT REJECTION REVEALS INSIGHTS INTO INTRAGRAFT TCR CLONALITY

Tiffany Shi[1,2,3], Ashley R. Burg[1,4], J. Timothy Caldwell[5], Krishna Roskin[1,6], Cyd M. Castro Rojas[1], P. Chukwunalu Chukwuma[7], George I. Gray[7], Sara G. Foote[7], Jesus Alonso[7#], Carla M. Cuda[8], David A. Allman[9], James S. Rush[10§], Catherine H. Regnier[10], Grazyna Wieczorek[10], Rita R. Alloway[11], Adele R. Shields[4], Brian M. Baker[7], E. Steve Woodle[4*], David A. Hildeman[1,2,3,12*]

[1]Division of Immunobiology, Cincinnati Children's Hospital Medical Center, Cincinnati, OH, USA
[2]Immunology Graduate Program, Cincinnati Children's Hospital Medical Center, Cincinnati, OH USA
[3]Medical Scientist Training Program, University of Cincinnati College of Medicine, Cincinnati, OH, USA
[4]Division of Transplantation, Department of Surgery, University of Cincinnati College of Medicine, Cincinnati, OH, USA
[5]Division of Nephrology and Hypertension, Cincinnati Children's Hospital Medical Center, Cincinnati, OH, USA
[6]Divison of Biomedical Informatics, Cincinnati Children's Hospital Medical Center, Cincinnati, OH, USA
[7] Department of Chemistry and Biochemistry and the Harper Cancer Research Institute, University of Notre Dame, Notre Dame, IN, USA
[8]Northwestern University, Feinberg School of Medicine, Department of Medicine, Division of Rheumatology, Chicago, IL, USA
[9]University of Pennsylvania Perelman School of Medicine, Philadelphia, Pennsylvania, USA
[10]Novartis Institutes for Biomedical Research, Immunology Disease Area, Basel, Switzerland
[11]Division of Nephrology and Hypertension, Department of Internal Medicine, University of Cincinnati College of Medicine, Cincinnati, OH, USA
[12]Department of Pediatrics, University of Cincinnati College of Medicine, Cincinnati, OH, USA
[#]current address: AbbVie, Inc., 1 N. Waukegan Rd. North Chicago, IL, USA
[§]current address: Kling Biotherapeutics BV, Amsterdam, The Netherlands
*authors contributed equally and share senior authorship

Conflict of Interest: This research was supported by Novartis.

Corresponding authors:
David A Hildeman, Cincinnati Children's Hospital Medical Center, 3333 Burnet Ave, Cincinnati, OH 45229, USA. Phone: 513-636-3923 email: david.hildeman@cchmc.org
E. Steve Woodle, University of Cincinnati College of Medicine, 3230 Eden Ave, Cincinnati, OH 45267, USA. Phone: 513-558-6001 email: woodlees@ucmail.uc.edu

Abstract

Bulk analysis of renal allograft biopsies (rBx) identified RNA transcripts associated with acute cellular rejection (ACR); however, these lacked cellular context critical to mechanistic understanding of how rejection occurs despite immunosuppression (IS). We performed combined single cell RNA transcriptomic and TCRα/β sequencing on rBx from patients with ACR under differing IS: tacrolimus, iscalimab, and belatacept. We found distinct $CD8^+$ T cell phenotypes (e.g., effector, memory, exhausted) depending upon IS type, particularly within clonally expanded cells ($CD8_{EXP}$). Gene expression of $CD8_{EXP}$ identified therapeutic targets that were influenced by IS type. TCR analysis revealed a highly restricted number of $CD8_{EXP}$, independent of HLA mismatch or IS type. Subcloning of TCRα/β cDNAs from $CD8_{EXP}$ into Jurkat76 cells ($TCR^{-/-}$) conferred alloreactivity by mixed lymphocyte reaction. Analysis of sequential rBx samples revealed persistence of $CD8_{EXP}$ that decreased, but were not eliminated, after successful anti-rejection therapy. In contrast, $CD8_{EXP}$ were maintained in treatment-refractory rejection. Finally, most rBx-derived $CD8_{EXP}$ were also observed in matching urine samples, providing precedent for using urine-derived $CD8_{EXP}$ as a surrogate for those found in the rejecting allograft. Overall, our data define the clonal $CD8^+$ T cell response to ACR, paving the next steps to improve detection, assessment, and treatment of rejection.

Introduction

Transplantation is the most effective treatment for kidney failure, providing improved survival and quality of life. To prevent rejection, patients are maintained on lifelong immunosuppression (IS) therapy, the standard-of-care being the calcineurin inhibitor (CNI) tacrolimus. Although current CNI-based regimens provide low acute rejection rates (~10%) in the first post-transplant year, thereafter patients remain at risk of therapeutically resistant late rejection that occurs at a rate of 1-3% per year. In addition, CNI-based regimens are associated with substantial toxicities due to off-target effects (1, 2). To avoid CNI toxicities, targeted IS agents that block T cell co-stimulation are being developed. Belatacept (CTLA4-Ig) is FDA-approved, and despite increased rejection rates 1-year post-transplant, long-term kidney function is increased under belatacept IS (3). However, belatacept-refractory rejection (BRR) episodes are more severe and more difficult to treat than rejection episodes that occur under CNI-based IS (4-6). Antibody-mediated blockade of the CD40/CD40L co-stimulatory pathway has shown promise as maintenance IS in non-human primates (7-9) and in pig-to-monkey xenografts (10-12). Fully human anti-CD40 monoclonal antibodies, such as iscalimab and bleselumab, have provided effective IS in human trials, but remained less efficacious compared to tacrolimus-based treatment in the prevention of organ rejection (13, 14). Thus, although co-stimulatory blockade approaches are promising, less toxic IS regimens, rejection occurring under these regimens remains poorly understood.

Alloreactive $CD8^+$ T cells present a major barrier to allograft acceptance as they are major drivers of acute cellular rejection (ACR) (15). Insights into graft-infiltrating T cells and their clonality during allograft rejection in previous studies were performed with

bulk TCR sequencing analyses (16-20). However, these studies only sequenced TCRβ chains, which, in absence of TCRα chain sequencing, do not indicate true clonality nor T cell type (e.g., $CD4^+$ or $CD8^+$). Similarly, bulk RNA sequencing (bulkseq) has identified rejection-associated transcripts (21-23), which contributed to the understanding of transplant rejection on the transcriptomic level. However, a major limitation of bulkseq analysis (both TCR and whole transcriptome) is that they do not attribute mRNA transcripts to individual cells, particularly T cells driving allograft rejection.

In contrast to bulkseq, single cell RNA sequencing (scRNAseq) has enabled transcriptomic analysis of individual cells (24). Additionally, single cell TCR sequencing (scTCRseq) enables assessment of T cell clonality (by single cell pairing of TCRα/β chains) in combination with scRNAseq (25). Although scRNAseq was used to characterize macrophages in a patient undergoing mixed rejection (26) and to define donor versus recipient leukocytes in patients undergoing antibody mediated rejection (27), single cell analysis of transcripts and $CD8^+$ T cell clonality in the acutely rejecting renal allograft remains undefined. Another study profiled bronchoalveolar lavage (BAL) fluid cells by scRNAseq from patients undergoing ACR of lung allografts before and after treatment with glucocorticoids (28). However, analysis of lung tissue during rejection was not performed, so the relationship of BAL fluid-derived T cells to T cells and other immune cells infiltrating lung allograft tissue during rejection remains unclear.

Here, we provide the first combined scRNAseq/scTCRseq analysis of human kidney allograft biopsies from patients undergoing ACR, including analyses of serial biopsies over time and comparative analyses of paired urine and allograft biopsy samples. Our analyses yield important new findings on the nature of human renal allograft rejection

including: (i) remarkable restriction of $CD8^+$ T cell clonal expansion; (ii) the type of maintenance IS affects gene expression within expanded $CD8^+$ T cell clonotypes ($CD8_{EXP}$) observed in index biopsies (biopsies obtained at time of rejection); (iii) persistence of $CD8_{EXP}$ observed in both index and subsequent renal allograft biopsies (even months later), reflecting long-term clonal persistence and adaptation despite rejection treatment; and (iv) correlation of $CD8_{EXP}$ observed in renal allograft rejection biopsies with those obtained in urinary sediment. Together, these results provide novel and fundamental insights into allograft rejection and how $CD8_{EXP}$ respond to anti-rejection therapies. Our results indicate that combined scRNAseq/scTCRseq has the potential to instruct the personalization and enhancement of anti-rejection therapy to improve long-term allograft survival.

Results

scRNAseq analysis of acutely rejecting human kidney allografts.

To understand ACR at the single cell level, we performed scRNAseq with 5' V(D)J sequencing on index kidney allograft biopsies obtained from 13 individual participants: 10 biopsies from participants undergoing an ACR episode and 3 control biopsies from participants not experiencing rejection. Hypothesizing that IS type may influence rejection phenotype, ACR samples included biopsies from 4 participants on tacrolimus, 3 on iscalimab, and 3 on belatacept maintenance IS (Table 1). Participants varied in terms of age, sex, race, etiology of end-stage renal disease, and donor type (living or deceased) and there were no significant differences in the number of HLA mismatches between IS groups (Supplemental Figure 1). Using our approach to collect

and freeze intact biopsies (29, 30) to allow for batch analyses and a novel cold-digestion protocol (31) to minimize temperature-driven artifacts in gene expression, biopsy-derived cells were subjected to scRNAseq. After alignment, quality control, and integration, uniform manifold approximation and projection (UMAP) analysis of all 13 index biopsies showed that cells were distributed across differing clusters with no clusters completely dominated by any particular sample (Figure 1A), indicating successful normalization and integration.

Initial cluster differentiation revealed 16 clusters of cells, including multiple immune and non-immune, kidney-derived cell populations. Cell types were identified based on differentially expressed genes and expression of canonical markers (32) (Supplemental Table 1). Within the immune cells, we observed γ/δ (clusters 0), $CD4^+$ (cluster 1), $CD8^+$ (clusters 2-4), including a population of proliferating $CD8^+$ and γ/δ (cluster 3) T cells; B cells (cluster 5); myeloid cells (clusters 6,7); and plasmacytoid dendritic cells (pDCs) (cluster 8) (Figure 1B). Of the kidney-derived cells, we identified proximal tubule (clusters 9-11), loop of Henle (cluster 12), distal tubule (clusters 13,15), and endothelial (cluster 14) cells (Figure 1B). Individual gene expression plots across clusters were consistent with cell cluster definitions. Immune cell clusters 0-8 expressed *PTPRC*, confirming that all immune clusters were comprised of leukocytes, as well as other cell type-defining markers, including *TRDC* (clusters 0), *CD4* (cluster 1), *CD8A* (clusters 2-4), *KLRK1* (clusters 0-4), *ITGAX* (cluster 0,7,8), *CD19* (cluster 5), and *CD14* (clusters 7,8) (Figure 1C). In humans *CD4* is also expressed by myeloid cells (33), which we also observed (clusters 7,8) (Figure 1C). As expected, no rejection biopsies were dominated by kidney-derived cells, while rejection biopsies had prodigious and

significantly increased amounts of immune infiltrates as compared to the no rejection samples (Figure 1, D and E), consistent with their rejection pathology score and histology (Supplemental Figure 2).

CD8$^+$ T cells dominate infiltrating immune cell populations in rejecting kidney allografts.

To further characterize immune infiltrates, immune cell clusters from the 10 index rejection biopsies were subsetted and re-analyzed. Subsequent cellular annotations revealed: 3 γ/δ T cell clusters, including effector (cluster 0), chronically stimulated (cluster 1), and resident memory (cluster 2) populations; 4 CD8$^+$ T cell clusters, including effector (cluster 3), resident memory (cluster 4); memory (cluster 5), and exhausted (cluster 6) populations; 3 CD4$^+$ T cell clusters, including follicular helper (cluster 7), memory (cluster 8), and Th17 (cluster 9) cells; 4 myeloid clusters, including macrophages (cluster 11), dendritic cells (cluster 12), extravascular monocytes (cluster 13); and plasmacytoid dendritic cells (pDCs) (cluster 14); 2 B cell populations, including naïve (cluster 15), and class-switched (cluster 16) B cells (Figure 2, A and B, Supplemental Table 2). Again, both CD8$^+$ and γ/δ T cells were present in a proliferating T cell population (cluster 10).

To examine the influence of maintenance IS regimens on immune cell types present within the allograft, cells were colored according to their IS regimens (tacrolimus [mustard], belatacept [blue], or iscalimab [pink]) **(**Figure 2C)**.** Although one participant on tacrolimus IS had a dominant influx of γ/δ T cells, most immune cell clusters were present at similar levels for all IS regimens (Figure 2D). Notably, all 10 samples are

dominated by T cells, with significantly more $CD8^+$ T cell infiltration compared to the rest of the immune cell subtypes (Figure 2D). Overall, maintenance IS type did not grossly affect overall immune cell composition of index biopsies.

Intragraft $CD8_{EXP}$ are heterogenous, expressing markers associated with of activation, exhaustion, and memory.

As $CD8^+$ T cells are primary drivers of ACR, analyses were refocused on just $CD8^+$ T cells from index biopsies in the 10 participants with ACR (Figure 3A). To get greater clarity of the cellular phenotypes associated with each cluster, we compared their differentially expressed genes (Supplemental Table 3) as well as expression of markers associated with T cell activation and effector function (*PRF1, GZMB, IFNG, HLA-DRA, CX3CR1, TBX21, MKI67*); exhaustion (*TOX, PDCD1, HAVCR2, LAG3, TIGIT, NR4A1, NKG7*); and memory (*ZNF683, PRDM1, CD69, ITGAE, CXCR6, S1PR1, SELL*) (Figure 3B). For example, in addition to their high-level expression of *PRF1* and *GZMB*, circulating memory cells ($CD8_{CIRCM}$), which includes both effector and central memory cells (34), in clusters 1 and 2 expressed high levels of *S1PR1* (Figure 3, A and B), which promotes their tissue egress (34, 35). Cells in clusters 2 and 4 were defined as resident memory cells ($CD8_{RM}$) based on their expression of *ZNF683, CD69,* and *CXCR6* (Figure 3, A and B), which are part of a tissue residency genetic program (36). In the kidney, not all resident memory cells express *ITGAE* (37, 38). $CD8_{RM}$ were further subdivided based on their differential expression of activation markers *GZMB*, *IFNG,* and *HLA-DRA* in cluster 4 relative to cluster 2 (Figure 3, A and B). Cells in clusters 3, 5, 6, and 7 were likely existing along a continuum of activation ($CD8_{ACTIV}$) and exhaustion

(CD8$_{EXH}$) based on their expression of markers associated with exhaustion (39) (*TOX, HAVCR2, PDCD1, TIGIT, LAG3)* and varying expression of activation/effector function genes (HLA-DR, *GZMB* and *IFNG)* (Figure 3, A and B). For example, cells in cluster 3, 5, and 7 may be more exhausted as they lack expression of *GZMB* and have lower levels of *IFNG* while cells in cluster 6 are more activated based on their higher expression of *GZMB* and *IFNG* (Figure 3, A and B). Finally, cluster 8 represents a population of proliferating CD8$^+$ T cells (CD8$_{PROLIF}$) based on expression of *MKI67* and other proliferation-associated genes (Figure 3, A and B, Supplemental Table 3). Thus, allograft-infiltrating CD8$^+$ T cells are heterogeneous with phenotypes consistent with circulating memory, resident memory, and varying states of activation, exhaustion, and proliferation.

Limited numbers of clonally expanded CD8$^+$ T cells are present in rejecting allografts.

CD8$^+$ T cell clonality within the rejecting allograft was determined using the 10X Genomics Chromium single cell 5' V(D)J platform. Full-length CDR3α/β sequences were obtained from ~90% of transcriptionally defined T cells and expanded clonotypes were defined as a CDR3α/β paired sequence present on >2 cells. Strikingly, we found a limited number of expanded CD8$^+$ clonotypes (CD8$_{EXP}$) across all 3 IS modalities (average of 20 unique CD8$_{EXP}$ per biopsy), while the majority of CD8$^+$ T cells were unexpanded (CD8$_{UNEXP}$) (Figure 3C). Further, there were no significant differences in the percentages or numbers of CD8$_{EXP}$ between IS modalities (Figure 3D). Intriguingly, CD4$^+$ clonal expansion was minimal, except for participants TAC_4 and ISCAL_2, which

had slightly higher proportions of expanded CD4+ T cells ($CD4_{EXP}$) (Supplemental Figure 3). Surprisingly, the level of clonal expansion was not correlated with the number of HLA mismatches, rejection grade, or absolute lymphocyte count (ALC) (Supplemental Figure 4). While T cells can express 2 TCRα chains, there was no significant difference in the percentage of T cells bearing two TCRα chains between the expanded (7.1%) and unexpanded (8.9%) clonotypes, indicating clonal expansion is driven by antigen recognition by cells expressing a single TCR.

To further understand the donor specificities of the $CD8_{EXP}$, we arbitrarily chose 5 $CD8_{EXP}$ CDR3α/β sequences from the scTCRseq data from one participant experiencing rejection (ISCAL_1) to subclone into Jurkat76 cells (a thymoma cell line lacking endogenous TCRα/β expression) (40). Resulting Jurkat76 transfectants were cultured with T cell-depleted PBMCs from the recipient's kidney donor or 3rd party cells and assayed for responses via IL-2 production. Strikingly, all 5 clones responded to donor, but not 3rd party, cells (Figure 3E) with significantly increased IL-2 production, confirming the alloreactivity of those $CD8_{EXP}$ identified in the rejecting kidney biopsy.

Maintenance IS type affects $CD8_{EXP}$ gene expression.

Interestingly, cluster distribution of $CD8_{EXP}$ varied based on maintenance IS. $CD8_{EXP}$ from tacrolimus-treated participants were distributed across all clusters but were more frequently represented in the $CD8_{RM}$ and $CD8_{EXH}$ populations (clusters 4, 5) than $CD8_{EXP}$ from belatacept- or iscalimab-treated participants (Figure 4, A and B). $CD8_{EXP}$ from iscalimab-treated participants predominantly resided in another $CD8_{EXH}$ population

(cluster 7) and the $CD8_{PROLIF}$ population (cluster 8), which was distinct from $CD8_{EXP}$ from belatacept- or tacrolimus-treated participants (Figure 4, A and B). $CD8_{EXP}$ from belatacept-treated participants clustered predominantly in both the $CD8_{CIRCM}$ (cluster 1) and $CD8_{ACTIV}$ (cluster 6) populations, consistent with prior work showing that belatacept-refractory rejection is associated with increased memory CD8+ T cells (5, 41). $CD8_{UNEXP}$ cells were most represented in clusters with the lowest levels of $CD8^+$ T cell activation ($CD8_{CIRCM}$, $CD8_{RM}$, and $CD8_{EXH}$) (Figure 4, A and B). Further examination of the differential gene expression between $CD8_{EXP}$ and $CD8_{UNEXP}$ from all samples revealed that $CD8_{EXP}$ had higher expression of *HLA* markers*,* activation and effector markers (*GZMH, GZMB*, *GNLY, PRF1, KLRD1, KLRG1, IFNG, ITGAE*), chemokines (*CCL3, CCL4*) and chemokine receptors (*CCL4L2*), and TNF family members *(TNFRSF9*) (Figure 4C). Thus, $CD8_{EXP}$ express alloreactive TCRs and have gene expression consistent with cells that have undergone TCR-mediated activation.

We next examined the differentially expressed genes (DEGs) in $CD8_{EXP}$ between the various IS modalities. $CD8_{EXP}$ from participants treated with iscalimab had increased expression of TNF family members such as *CD27, TNFRSF9,* and *CD70* (blue), as well as *FKBP1A* (red), an intracellular tacrolimus binding protein. Interestingly, *FKBP1A* expression is decreased in $CD8_{EXP}$ under tacrolimus and belatacept IS (Figure 4D)**.** In contrast, $CD8_{EXP}$ from participants treated with belatacept show upregulation of activation markers such as *GNLY, GZMH,* and *GZMB* when compared to iscalimab and tacrolimus $CD8_{EXP}$ (Figure 4D).

Previously, our group demonstrated increased mTOR activity in peripheral blood $CD8^+$ T cells in patients with ACR under belatacept, but not tacrolimus, and treatment of

belatacept-refractory ACR with everolimus mitigated their ACR (5). Based on this, we performed a supervised analysis of mTOR pathway-related genes in the $CD8_{EXP}$ under the 3 maintenance IS regimens (Figure 4E). Notably, $CD8_{EXP}$ from participants under belatacept IS showed not only a significantly increased expression of mTOR complex genes (*mTOR, RPTOR, and RICTOR*), but also a decreased expression of 2 negative regulators of mTOR activation (*TSC1, TSC2*). This contrasts with $CD8_{EXP}$ from participants under tacrolimus or iscalimab based IS which showed lower levels of *RPTOR* and *RICTOR* and relatively higher levels of *TSC1* and *TSC2*. Combined, these data indicate that rejections arising under differing IS are associated with varying gene expression of potential therapeutic targets.

$CD8_{EXP}$ clonal populations may expand, contract, or persist in response to anti-rejection treatment.

We next examined the persistence of $CD8_{EXP}$ clonal populations after anti-rejection therapy. Participant TAC_3 experienced an index Banff ACR 1B rejection on post-transplant day (PTD) 217, which was treated with rabbit anti-thymocyte globulin (rATG) and prednisolone (Table 2). Two weeks later (PTD 232), a follow-up biopsy revealed histologic improvement to Banff borderline lesion and a substantial decrease in the total numbers of $CD8^+$ T cells. Intriguingly, scRNAseq analysis revealed an increase in the frequency of $CD8_{EXP}$ from 7.7% (26 out of 336 total clonotypes) in the index biopsy to 13.2% (24 out of 182) (Figure 5A). Out of the 24 $CD8_{EXP}$ that were identified at PTD 232, 10 were identical to those present as $CD8_{EXP}$ in the index biopsy (PTD 217) (Figure 5A). An integrated analysis of all 3 timepoints revealed 7 $CD8^+$ T cell clusters,

including 1 $CD8_{RM}$ (cluster 0), $CD8_{CIRCM}$ (clusters 1,2), $CD8_{EXH}$ (cluster 3), 2 $CD8_{ACTIV}$ (clusters 4, 5), and $CD8_{PROLIF}$ (cluster 6) (Figure 5, B and C, Supplemental Table 4). On the index biopsy, most $CD8_{EXP}$ were $CD8_{ACTIV}$ (clusters 4,5) and $CD8_{PROLIF}$ (cluster 6). Rejection treatment with rATG and corticosteroids resulted in marked reduction in $CD8_{ACTIV}$ (clusters 4,5) and $CD8_{PROLIF}$ (cluster 6) $CD8_{EXP}$ (Figure 5D, Supplemental Table 4). Notably, at PTD 232, a dominant $CD8_{EXP}$ population with a $CD8_{RM}$ phenotype (cluster 0) appeared. Nine weeks later (PTD 295), another biopsy revealed no histologic rejection, and a loss of the $CD8_{RM}$ phenotype (cluster 0), further reduction in $CD8_{ACTIV}$ (clusters 4,5) and $CD8_{PROLIF}$ (cluster 6), but a small increase in $CD8_{EXH}$ (cluster 3). scTCRseq analysis revealed 5 distinct $CD8_{EXP}$, 3 of which were from previous biopsies (Figure 5, A and D). DEG analysis between the $CD8_{EXP}$ from the 3 timepoints revealed that $CD8_{EXP}$ from the index rejection biopsy (PTD 217) expressed effector function genes (*GZMB, GZMK, GNLY)* but also exhaustion markers (*LAG3, HAVCR2, TIGIT),* while clonotypes two weeks later (PTD 232) displayed resident memory genes (*ZNF683, CD69, ITGAE)* and clonotypes two months later (PTD 295) expressed *GZMK*, *KLRB1*, as well as chemokines *XCL1, XCL2* (Figure 5E). Thus, even though histologic rejection resolved, $CD8_{EXP}$ persisted at 11 weeks after initial rejection despite rATG and corticosteroid anti-rejection treatment.

We also followed participant BELA_1, where a biopsy on PTD 111 revealed a Banff ACR 2A rejection under belatacept-based IS. This rejection episode was treated with rATG and corticosteroids (Table 2), and two weeks later (PTD 125), a follow-up biopsy revealed improvement to a borderline lesion. Interestingly, despite histological improvement and a decreased in the number of $CD8_{EXP}$ from PTD 111 (8 $CD8_{EXP}$) to

PTD 125 (4 $CD8_{EXP}$), the frequency of total clonotypes and number of expanded cells were similar between the two timepoints (Figure 6A). Of the 4 $CD8_{EXP}$ identified at PTD 125, 1 was previously identified from PTD 111 while 3 were newly expanded at PTD 125 (Figure 6, A and D). An integrated analysis of CD8+ T cells from both timepoints reveal 5 distinct clusters, including $CD8_{RM}$ (cluster 0), $CD8_{ACTIV}$ (clusters 1, 3), $CD8_{EXH}$ (cluster 2), and $CD8_{PROLIF}$ (cluster 4) (Figure 6, B and C, Supplemental Table 5). In-depth analysis of the gene expression of $CD8_{EXP}$ following anti-rejection treatment with rATG and corticosteroids revealed surprisingly limited changes in DEGs despite histologic improvement to a borderline lesion.

Participant ISCAL_1 presented with a Banff ACR 2A rejection under iscalimab-based IS at one-month post-transplant that was treated with rATG and a corticosteroid taper for persisting Banff 1B rejection. A biopsy obtained on PTD 60 revealed a Banff 1A rejection (Table 2), and scTCRseq analysis revealed 35 individual $CD8_{EXP}$. Tacrolimus-based anti-rejection treatment was initiated, and a biopsy obtained 2.5 weeks later (PTD 78) demonstrated no rejection and significantly reduced $CD8_{EXP}$. However, there was no change in the frequency of $CD8_{EXP}$ (6.5% at the first timepoint and 6.3% at follow-up), and nearly half of the $CD8_{EXP}$ were identical to those in the first biopsy (Figure 7, A and D). Following rejection resolution, tacrolimus was tapered. A repeat biopsy obtained approximately 1 year later (PTD 336) revealed histologic resolution of rejection, and only 1 $CD8_{EXP}$ persisted from the initial timepoint (PTD 60) (Figure 7, A and D). An integrated analysis of $CD8^+$ T cells from all 3 timepoints identified 6 clusters: $CD8_{RM}$ (cluster 0), $CD8_{EXH}$ (clusters 1, 3), $CD8_{ACTIV}$ (clusters 2, 4) and $CD8_{PROLIF}$ (cluster 5). Most of the $CD8_{EXP}$ identified from PTD 60 were present as

$CD8_{ACTIV}$ (cluster 4) and $CD8_{PROLIF}$ (cluster 5) with a few as $CD8_{RM}$ (cluster 0) and a few as $CD8_{EXH}$ (cluster 1) (Figure 7, B and C, Supplemental Table 6). Strikingly, at PTD 78, nearly all $CD8_{EXP}$ that were $CD8_{ACTIV}$ (cluster 4) were decreased and a substantial number of those clones were now present as $CD8_{EXH}$ (cluster 3) (Figure 7, B and C, Supplemental Table 6). Notably, despite rejection resolution at PTD 336, the one remaining $CD8_{EXP}$ first identified from rejection at PTD 60 had a $CD8_{RM}$ phenotype (evidenced by *ZNF683* expression) (cluster 0) (Figure 7E). Notably, the TCR expressed by this clone was one of the TCRs defined as alloreactive (Figure 3D). This demonstrates that, despite resolution of rejection, alloreactive $CD8^+$ T cell clones can persist for at least a year within the histologically normal allograft.

A fourth participant, ISCAL_3, was diagnosed with a Banff 1B rejection at 20 weeks post-transplant (PTD 137) (Table 2) while on iscalimab maintenance IS, and scTCRseq analysis revealed 7 distinct $CD8_{EXP}$ (Figure 8A). Interestingly, scTCRseq analysis of urine sediment at the same timepoint contained 11 $CD8_{EXP}$, 4 of which were identical to the $CD8_{EXP}$ in the biopsy (Figure 8, B and C). To treat their rejection, the participant was converted to tacrolimus IS, given a prednisolone pulse, and iscalimab was discontinued. Two weeks later (PTD 151), a repeat biopsy revealed Banff ACR 1B rejection (Table 2) and an increase in the $CD8_{EXP}$ clonal frequency (4.7% to 7.2%). Importantly, each $CD8_{EXP}$ present in the index biopsy were also observed in the second biopsy, and 16 $CD8_{EXP}$ were found in both the biopsy and urine samples (Figure 8, A-C). Four weeks later (PTD 179), repeat biopsy revealed a borderline lesion (Table 2), with a continued persistence of $CD8_{EXP}$ (6.3%) (Figure 8A). Approximately 72% (13 out of 18) $CD8_{EXP}$ in the PTD 179 biopsy had been observed in prior biopsies and a similar

persistence of $CD8_{EXP}$ was observed in the urine (Figure 8, A and B). An approximate 50% overlap in $CD8_{EXP}$ were noted in both biopsy and the urine at PTD 179 (Figure 8C). Four months later (PTD 291), the participant was diagnosed with a Banff 1B mixed acute rejection. scTCRseq again demonstrated persistence of $CD8_{EXP}$ at a frequency 9.5% of all clonotypes (16 out of 168) and roughly half of these were observed in earlier biopsies (Figure 8C). Overall, these data show that in addition to persistent $CD8_{EXP}$ in the rejecting allograft despite anti-rejection therapy, persistent $CD8_{EXP}$ can also be observed in the urine, and urine $CD8_{EXP}$ reflect those found in the graft.

An integrated analysis of allograft-resident $CD8^+$ T cells from all 4 timepoints revealed 7 clusters, including $CD8_{RM}$ (cluster 0), $CD8_{CIRC}$ (cluster 1), $CD8_{EXH}$ (cluster 2), $CD8_{ACTIV}$ (clusters 3-5), and $CD8_{PROLIF}$ (cluster 6) (Figure 9, A and B, Supplemental Table 7). Most $CD8_{EXP}$ from the index biopsy (PTD 137) had gene expression consistent with $CD8_{ACTIV}$ (clusters 4,5) and $CD8_{PROLIF}$ (cluster 6) (Figure 9, A-C), and after addition of tacrolimus and corticosteroids for anti-rejection therapy, most $CD8_{EXP}$ from the second biopsy (PTD 151) were identified as $CD8_{CIRCM}$ (cluster 1) and $CD8_{ACTIV/EFF}$ (clusters 4,5) (Figure 9, A-C). Mycophenolate mofetil (MMF) was added to the maintenance IS regimen and another biopsy taken at PTD 179. The majority of $CD8_{EXP}$ at this timepoint appeared to have shifted their gene expression and were identified as $CD8_{EXH}$ cells (cluster 2), with some cells having a $CD8_{CIRCM}$ (cluster 1) and a $CD8_{RM}$ (cluster 0) phenotype (Figure 9, A-C). Finally, at PTD 291 following tapering of MMF, a new clonotype appeared and localized to cluster 0, a cluster populated by only a few cells in the earlier samples and whose gene expression profile was consistent with a pathogenic $CD8_{RM}$ phenotype (cluster 0), showing high levels of *ZNF683* and

CD160 (Figure 9, C and D). Taken together, these data show that, during unresolved rejection, treatment with tacrolimus, corticosteroids, and MMF failed to eliminate $CD8_{EXP}$ instead was associated with substantial changes in their gene expression.

DISCUSSION

Using single cell genomics, we uncovered an unexpectedly small number of $CD8_{EXP}$ present in renal allograft biopsies undergoing rejection. This seemingly contrasts prior data using bulk TCRβ sequencing approaches of kidney allograft biopsies (16, 17, 20, 42). We envision a few explanations for these differences. First, transplant patients are often lymphopenic due to induction therapy, which could severely limit the available repertoire. Although we found that patients with a normal absolute lymphocyte count had low numbers of $CD8_{EXP}$, it remains possible that induction therapy drives a long-lasting reduction of the available repertoire. Second, while it is possible that many $CD8_{UNEXP}$ are alloreactive, we think this unlikely as our longitudinal analysis showed that very few $CD8_{UNEXP}$ ended up as $CD8_{EXP}$ in subsequent biopsies. Third, alloresponses may involve immunodominance mechanisms. For example, perhaps the nature of the T cell (i.e., pre-existing memory or TCR avidity) allows a limited number of clonotypes to outcompete for resources and dominate the response. Further work determining TCR specificity of $CD8_{EXP}$ and their presence in naïve and memory T cell populations prior to transplantation will help distinguish between these possibilities.

In this regard, our platform of subcloning of TCRs into Jurkat76 cells and testing them against donor versus third-party T cell-depleted PBMCs will be useful to study the

biology of allospecific TCRs. In addition to linking TCR specificity to cell phenotype, screening combinatorial peptide libraries (CPLs) will enable the identification of peptides bound to donor HLA recognized by allospecific TCRs. This is important because a lack of an ability to track and monitor allospecific T cells has been a major impediment to understanding their development and function. Further, as many have suggested, a large fraction of allospecific T cells may be pre-existing memory cells with specificities to pathogens previously encountered (43, 44). Similarly, use of *recipient* PBMCs and CPLs will allow for identification of TCRs with potential cross-reactivity. As such, future extensions of these studies have the potential to yield insights into the fundamental nature of allorecognition, whether alloreactive TCRs focus on HLA epitopes versus peptide, and protein structure/function analysis of TCR CDR3/HLA/peptide interactions. In addition, additional work will be necessary to determine the function of graft-resident T cells and further connect transcriptomic phenotype with function and potentially with specificity.

Our data also showed that the type of IS affected the gene expression and phenotype of $CD8_{EXP}$. Importantly, scRNAseq provided the resolution to identify potential therapeutic targets that may be exploited for optimal anti-rejection therapy. For example, we previously reported that patients undergoing BRR responded to treatment with everolimus (5). Our data here are consistent with an underlying mechanism for this prior observation as $CD8_{EXP}$undergoing BRR have elevated expression of mTOR components *RICTOR* and *RPTOR*. Similarly, increased expression of *FKBP1A* in iscalimab-refractory rejection suggests that such rejections may be sensitive to tacrolimus. Thus, such analysis could provide physicians with informed and personalized approaches to optimize anti-rejection therapies.

We also found that $CD8_{EXP}$ can persist in the kidney allograft for months, despite successful anti-rejection therapy, confirming and extending prior MLR studies in peripheral blood (16). Interestingly, we also found that individual $CD8_{EXP}$ surviving rejection therapy adapt, and possibly survive, by altering gene expression (i.e., adopting a $CD8_{RM}$ phenotype) in response to anti-rejection therapy. This incomplete $CD8_{EXP}$ elimination and persistence may underlie recurrent rejection and/or long-term smoldering allograft injury, contributing to rejection-associated reduction in allograft survival. Additional work is required to determine the persistence and specificity of TCRs of $CD8_{EXP}$ from participants undergoing anti-rejection therapy and whether these $CD8_{RM}$ cells are associated with protective (45) versus pathologic (46) responses. An intriguing point remains – whether complete elimination of $CD8_{EXP}$ will significantly improve the poor allograft survival rates that are observed following treatment of moderate and severe ACR. Addressing this issue may represent a major advance in rejection therapy.

Our observation that clonally identical $CD8_{EXP}$ are found in the urine and biopsy is likely a result of $CD8^+$ T cell killing of renal tubular epithelial cells, underlying the predominant histologic feature of ACR (tubulitis). In tubulitis lesions, $CD8_{EXP}$ likely traverse the renal tubular basement membrane and gain access to the urinary space, in contrast to those remaining in the interstitial space. We are currently determining the number and gene expression of $CD8_{EXP}$ in the urine and whether this correlates with the degree of tubulitis. Interestingly, for participant ISCAL_3, the $CD8_{EXP}$ with a $CD8_{RM}$ phenotype was present only in the biopsy (not urine), suggesting their retention in the kidney precluded their ability to traverse the basement membrane.

While we focused on $CD8^+$ T cells, many other cell types are amenable to similar analysis. In this light, there was 1 participant (TAC_1) with a substantial influx of $\gamma\delta$ T cells, and although it is possible that this massive influx of $\gamma\delta$T cells could be due to CMV viremia (47, 48), this patient was CMV+ but was never demonstrated to have CMV viremia. Further, we note that despite an exhaustive search, we have not been able to confidently identify a population of NK cells in our samples, as we cannot be confident any identified population are not $\alpha\beta$ or $\gamma\delta$ T cells that were dropouts for TCR expression. As such, in-depth analyses of other immune cell and kidney-derived cell populations currently underway utilizing the same samples described herein. In addition, other single cell genomics-based approaches, including spatial transcriptomics (ST) and ATACseq. ST will place the cell populations identified by scRNAseq in their histologic context, while ATACseq may further refine and expand our knowledge of gene regulatory networks active in various cell types.

In summary, scRNAseq analysis of human renal allograft rejection reveals highly restricted $CD8_{EXP}$ that exhibit alloreactivity and varying responses to rejection therapy, including their persistence despite rejection resolution. Importantly, these $CD8_{EXP}$ vary in gene expression based on the nature of maintenance IS. These novel and fundamental insights delineate approaches for developing innovative individualized rejection therapies that can be tested in carefully designed clinical trials.

METHODS

Sample Collection

Tissue samples were collected directly during the biopsy procedure using an 18g biopsy needle and placed immediately in HypoThermosol FRS Preservation Solution (HTS; BioLife Solutions Inc, 101102) on ice. When applicable, clean-catch urine samples were collected and spun down at 300xg to obtain the cellular components. Both sample types were frozen at -80°C in CryoStor CS10 (BioLife Solutions Inc, 210102) in a Mr. Frosty Freezing Container (Nalgene 5100-0001), then stored in liquid nitrogen until ready for analysis.

Tissue Dissociation

Tissue dissociation protocol was modified from a previously described cold-active protease digestion(31). Kidney core biopsies were slowly thawed, cut into 1-2mm pieces, then subject to gentle cold digestion on ice using 10% FBS-supplemented RPMI media containing 100mg/mL trypsin inhibitor from soybean (Roche, 10109886001), 10mg/mL collagenase A from clostridium histolyticum (Roche, 10103586001), 10mg/mL collagenase type IV from clostridium histolyticum (Worthington, LS004186), 250U DNase I (Roche, 4536282001), and 5mM $CaCl_2$. Digestion was performed twice at 10 minutes each, with intermittent rotating and gentle pipet mixing with wide orifice tips. The digested tissue was passed through a pre-primed 30mm cell strainer, breaking up any remaining visible tissue using a rubber syringe plunger. The single cell suspension was passed through a second pre-primed 30mm cell strainer, then centrifuged at 300xg at 4°C for 5 minutes. Viability and live cells were counted by trypan blue exclusion then resuspended at 1000 cells/mL, per the 10X Genomics Chromium protocol. The cells, kept on ice, were immediately prepared for single-cell barcoding.

Single cell barcoding, cDNA synthesis and library preparation

All samples were processed for single-cell sequencing following the Chromium Next GEM Single Cell V(D)J Reagent Kits v1.1 protocol. Briefly, cells were uniquely barcoded by using 10X fluidics (10X Genomics Chromium Single Cell Controller) to combine each individual cells with an individual barcoded Single Cell 5' Gel Bead creating a Gel Beads-in-emulsion (GEMs) solution (10X Genomics, PN-1000165 and PN-1000120). An average of 17,400 cells were loaded to achieve an estimated 10,000 cell recovery. GEM gel beads were dissolved, and cDNA was synthesized from the resulting tagged mRNA transcripts over 14 amplification cycles. 50ng of cDNA was used for the construction of each library. Total gene expression libraries (PN-1000020) and libraries of enriched TCR sequences (PN-1000005) were created using the Single Index Kit Set A (PN-1000213).

Sequencing, alignment, and generation of matrices

Total gene expression and TCR sequence-enriched libraries were sequenced on the NovaSeq 6000 sequencer using S1, S2 or S4 flow cells, with the goal to obtain >320M reads per sample. Raw base call files were de-multiplexed with Cell Ranger (version 6.1.2) using mkfastq. Reads were aligned to human reference genome (version GRCh38) and gene expression quantified against GENCODE (release 32) using the count function of CellRanger. Genomics data is available via the NCBI BioProject, accession number PRJNA974568.

Single-cell RNASeq analysis pipeline

Single-cell analysis was carried out with R (version 4.2.0) running inside RStudio (version 4.1.1) using Seurat (version 4.1.0)(49, 50). Cells expressing more than 25% mitochondrial gene transcripts or fewer than 200 genes, including additional low-quality cells, were excluded from the analysis. TCR alpha and beta gene variants were collapsed as singular 'tcr-alpha' and 'tcr-beta' genes, respectively. Gene expression counts were normalized with the NormalizeData function in Seurat. The samples were integrated using FindIntegrationAnchors and IntegrateData functions from Seurat. This integrated data set was used for principal component analysis, variable gene identification, Shared Nearest Neighbor (SNN) clustering analysis, and creation of UMAP. Metadata was updated to include identities of TCR clonotypes and those categorized as expanded and unexpanded, as described below. Differentially expressed genes were determined using FindMarkers, with a logfc threshold of 1 and minimum percent expression of 0.2. Genes that were differentially expressed at an adjusted p-value < 0.05 were used for analyses.

TCR clonal analysis

Cell Ranger outputs for the TCRα/β sequencing data were merged into the Seurat metadata for various integrated analyses. Filtered_contig_annotations.csv and clonotypes.csv files were used to obtain CDR3α/β information linked to individual barcodes, which were then merged with barcodes from the Seurat metadata to combine scRNAseq analysis with scTCRseq analysis. $CD8^+$ cells were identified from the immune cell populations through subsetting of $CD8^+$ clusters and removal of cells expressing *CD4*, *TRDC*, and *CD68*. Clonotypes with identical CDR3α/β sequences present in >2 cells

(identified through unique barcodes) were determined to be expanded. Clonotypes with 2 CDR3β chains or only an individual CDR3α or CDR3β chain were classified as unexpanded. Analysis of the merged Seurat metadata allowed determination of numbers of CD8+ barcodes, total numbers of clonotypes, and numbers of $CD8_{EXP}$ and $CD8_{UNEXP}$ clonotypes.

To determine the position of $CD8_{EXP}$ clonotypes on UMAPs, expanded clonotypes were recalled using their clonotype_id and set as a new identity on the plots. Overlapping clonotypes between biopsy and urine samples were done using the package VennDiagram, and clonotype tracking over sequential timepoints was done using the package Immunarch (51) v0.9.0 with modified input files to reflect only $CD8^+$ cells in the analysis.

TCR-expressing Jurkats

$TCR\alpha/\beta^{-/-}$ Jurkat 76 cell lines were provided by Dr. Michael Nishimura (Loyola University, Chicago, IL). Jurkat76 cells stably expressing the TCRs of interest were generated by transfection using the Neon Transfection System (Thermo Fisher). The cells were transfected with the pCMV(CAT)T7-SB100 plasmid and the pSBbi-Neo Sleeping Beauty vector containing the full length TCR α and β chains (obtained from scTCRseq of 1 participant [ISCAL_1] undergoing rejection) separated by the P2A self-cleaving peptide as previously described (52). After electroporation, the cells were maintained in RPMI media (RPMI 1640 with 10% FBS, 100 units/mL penicillin, and 100 µg/mL streptomycin). and were incubated at 37°C and 5% CO_2. Cells expressing the TCR of interest were selected for by using media containing 1.2mg/mL of G418 (Geneticin™, ThermoFisher

10131027). Cells were analyzed and sorted for transfection efficiency via flow cytometry analysis using anti-human CD3 APC/Cy7-conjugated antibody and anti-human CD34 PE-conjugated antibody for TCR-expressing cells (BioLegend, 300426 at 10 µg/mL and BioLegend, 343606 at 1.25 µg/mL).

Cell Culture and ELISAs

TCR-expressing Jurkat76 cells were cultured overnight (20 hours) in PMA-supplemented non-selection RPMI media at a 1:1 ratio with either T cell-depleted PBMCs derived from the participant's donor or derived from a third-party healthy donor. Co-cultures were performed as distinct triplicates (n=3). Co-culture supernatant was collected following completion of culture and analyzed for IL-2 using the ELISA MAX^{TM} Deluxe Set for human IL-2 (Biolegend, 431804) at a dilution of 1:5.

Study Approval

All participants were independently enrolled in this mechanistic rejection study approved by the University of Cincinnati Institutional Review Board (IRB 2017-4696, 2019-0469). One group of patients were simultaneously enrolled in the CIRRUS I trial (NCT03663335). Enrollment occurred at two Cincinnati, Ohio hospitals (University of Cincinnati Medical Center or The Christ Hospital) upon scheduling of a for-cause renal allograft biopsy. All participants provided written informed consent before study procedures occurred, with continuous consent ensured throughout participation.

Statistics

Statistical analyses, including t-tests, one-way ANOVA analyses, and linear regressions, were done using GraphPad Prism version 9.3.1. Significance was calculated, adjusting for multiple comparisons, at $p<0.05$. Differential gene expression analyses were performed using Seurat (version 4.1.0) function FindAllMarkers to identify significantly expressed genes at $p<0.05$.

Author Contributions:

TS, ARB, BMB, ESW, DAH designed research studies, TS, ARB, CMCR, PCC, GIG, SGF, JA conducted experiments, ARB, RRA, ARS, ESW recruited participants, TS, ARB, JTC, KR, PCC, GIG, JA, CMC, DAA, JSR, CHR, GW, BMB, ESW, DAH analyzed data, BMB provided reagents, and TS, ARB, JTC, JSR, CHR, GW, BMB, ESW, DAH wrote and edited the manuscript.

Acknowledgements:

We graciously thank all the participants, participant families, and other participant support persons that have made these studies possible. We would like to acknowledge the University of Cincinnati (UC) Transplant Research Team and the UC and Christ Hospital Transplant Care Team for their hard work in consenting, following, and caring for research participants. We acknowledge the UC Pathology team, in particular Dr. Paul Lee, for their contributions to the pathological and histological analyses. We thank Dr. Steve Potter and Andrew Potter for their help with development of the cold protease digestion protocol. We would also like to thank the UC/CCHMC Center for Transplant Immunology for their guidance and support in this project.

This research was also made possible, in part, using the Cincinnati Children's Single Cell Genomics Core [RRID:SCR_022653], DNA Sequencing and Genotyping Core [RRID:SCR_022630], and Biomedical Informatics Core. We specifically acknowledge the assistance of Kelly Rangel and Shawn Smith from the Single Cell Genomics Core. This work was supported by a grant from Novartis and from Public Health Service grants AI167482 (T.S.), AI142264 (D.A.H, E.S.W.), UH2AR067688 (D.A.H., E.S.W.), UL1TR000077 (D.A.H., E.S.W.), AI169863 (D.A.H., E.S.W., and B.M.B.)

Figure Legends

Figure 1. Single cell RNA sequencing analysis of transplanted kidney allografts. Single cell suspensions from thirteen different biopsies (3 without rejection, 10 with rejection) were individually subjected to 5' single cell RNAseq on the 10X platform with V(D)J sequencing. After alignment using Cell Ranger, cells with >25% mitochondrial content and <200 genes, including additional low-quality cells, were removed, and samples were integrated using Seurat. **(A, B)** UMAP plots displays cell contribution by sample and cell type. **(C)** Expression of "signature" genes across cell types. Blue color intensity reflects the expression level of individual genes within given cells. **(D)** Separation of samples based on rejection status. UMAP plots show cells from no rejection samples (gray, left plot) versus rejection samples (pink, right plot). **(E)** Frequency of cell types within each sample are displayed in bar graphs. Statistical analyses reveal a significantly increased proportion of immune infiltration in the rejection samples (n=10) as compared to the no rejection samples (n=3) [two-tailed t-test, ****p<0.0001].

Figure 2. Diverse immune cell infiltrate during kidney allograft rejection. Index samples from the 10 participants undergoing rejection were integrated, clusters annotated as non-immune cells were removed, and the data were re-normalized and re-clustered using Seurat. **(A)** UMAP plot shows immune cell clusters and accompanying annotations. **(B)** Violin plots display the relative gene expression level of indicated genes across each cluster. **(C)** Samples were segregated according to maintenance IS type. UMAP plots shows immune cell clustering of samples from participants with rejection under tacrolimus (left plot, shades of mustard); belatacept (middle plot, shades of blue); or iscalimab (right plot, shades of pink) maintenance immunosuppression **(D)** Frequency of cell types within each sample are displayed in bar graphs. Statistical analyses revealed a significantly increased proportion of CD8+ T cells in the immune infiltration as compared to other immune subtypes (n=10) [one-way ANOVA, ***p<0.0006, **p<0.007].

Figure 3. Analysis of infiltrating $CD8^+$ T cells in kidney allograft rejection. $CD8^+$ clusters from the immune cells analysis were identified for further analyses; $CD4^+$ and γ/δ T cells were removed. The samples were then re-analyzed using Seurat. **(A)** UMAP plot shows cell type annotations based on differentially expressed genes. **(B)** Violin plots show relative expression level of indicated genes selected to characterize cell cluster phenotypes as activated, exhausted, and memory. **(C)** Pie charts display number and frequency of expanded CD8+ clonotypes ($CD8_{EXP}$) found in the biopsy during rejection by participant sample, based on their unique CDR3α/β sequences.

Expanded clonotypes are defined as having >2 cells with identical CDR3α/β sequences. Different colors represent individual expanded clonotypes (gray area represents unexpanded clonotypes) and the size of the colored area represents the relative size of the expanded clonotypes. **(D)** The percentage (left graph) and total number (right graph) of $CD8_{EXP}$ in each treatment group (tacrolimus n=4, belatacept n=3, iscalimab n=3) are displayed in the bar graphs (+/- SD) [one-way ANOVA, ns = not significant, p>0.05]. **(E)** Full length TCRs with unique CDR3α/β sequences derived from 5 $CD8_{EXP}$ from one participant experiencing rejection (ISCAL_1) were subcloned into individual Jurkat76 cells. Individual clones were cultured in triplicate either alone, with donor or with 3rd party T cell-depleted PBMCs for 20 hours and IL-2 levels in the supernatant measured via ELISA. Results show the level of IL-2 in pg/ml for each condition (+/- SD) done in triplicates (n=3) [one-way ANOVA, *p<0.05].

Figure 4. Gene expression differences in $CD8_{EXP}$ between tacrolimus, belatacept, and iscalimab maintenance IS. (A) Clustering of $CD8_{EXP}$ based on maintenance IS type. UMAP plots show clustering of $CD8_{EXP}$ (colored dots) versus $CD8_{UNEXP}$ (gray dots) from participants under either tacrolimus (left plot, shades of mustard); belatacept (right plot, shades of blue); or iscalimab (middle plot, shades of pink) maintenance IS. **(B)** Bar graphs display the fraction of expanded clonotypes (tacrolimus, belatacept, or iscalimab) and unexpanded clonotypes contributing to each $CD8^+$ T cell cluster. **(C)** Violin plots show the relative expression of indicated genes in expanded ($CD8_{EXP}$) and unexpanded ($CD8_{UNEXP}$) $CD8^+$ clonotypes. **(D)** Heatmap displays (average) expression of unsupervised differentially expressed genes (p<0.05) in $CD8_{EXP}$ under tacrolimus

(n=4), belatacept (n=3), and iscalimab (n=3) maintenance IS. Blue text denotes 3 TNF family member genes and red text denotes *FKBP1A*, a target of tacrolimus. **(E)** Heatmap displays a supervised analysis of the average expression of mTOR pathway-related genes in $CD8_{EXP}$ from participants under tacrolimus, belatacept, and iscalimab maintenance IS.

Figure 5. Temporal scRNAseq analysis of the response to anti-rejection therapy under tacrolimus maintenance immunosuppression (IS). A participant on tacrolimus IS (TAC_3) was diagnosed with ACR 1B on post-transplant day (PTD) 217 and a biopsy was obtained prior to anti-rejection treatment with rATG and steroids. A second biopsy was obtained on PTD 232 and the participant was diagnosed with a borderline lesion. A third biopsy was taken at PTD 295 and the participant was diagnosed with no rejection. **(A)** Pie charts display number and frequency of expanded clonotypes found in the index biopsy (PTD 217) and subsequent follow-up biopsies (PTD 232, PTD 295). Bar graph shows overlapping clonotypes across the 3 timepoints. **(B)** UMAP shows $CD8^+$ clusters in an integrated analysis of all timepoints. **(C)** Violin plots show relative expression level of indicated genes selected to characterize cell cluster phenotypes as activated, exhausted, and memory. **(D)** Temporal analysis of $CD8_{EXP}$ following anti-rejection therapy. UMAP plots show clustering of expanded ($CD8_{EXP}$, colored dots) versus unexpanded ($CD8_{UNEXP}$, gray dots) $CD8^+$ clonotypes from the participant at PTD 217 (left plot); PTD 232 (middle plot); or PTD 295 (right plot). $CD8_{EXP}$ first expanded on PTD 217 are shown in pink, those first expanding on PTD 232 are shown in green, and those first expanding on PTD 295 are shown in blue. **(E)** Heatmap shows average expression

of unsupervised differentially expressed genes ($p<0.05$) found between $CD8_{EXP}$ at each timepoint.

Figure 6. Temporal scRNAseq analysis of the response to anti-rejection therapy under belatacept maintenance immunosuppression (IS). A participant on belatacept IS (BELA_1) was diagnosed with ACR 2A on post-transplant day (PTD) 111 and a biopsy was obtained prior to anti-rejection treatment with rATG and steroids. A second biopsy was obtained on PTD 125 and the participant was diagnosed with a borderline lesion. **(A)** Pie charts display number and frequency of expanded clonotypes found in the index biopsy (PTD 111) and the subsequent follow-up biopsy (PTD 125). Bar graph shows overlapping clonotypes across the 2 timepoints. **(B)** UMAP shows $CD8^+$ clusters in an integrated analysis of both timepoints. **(C)** Violin plots show relative expression level of indicated genes selected to characterize cell cluster phenotypes as activated, exhausted, and memory. **(D)** Temporal analysis of $CD8_{EXP}$ following anti-rejection therapy. UMAP plots show clustering of expanded ($CD8_{EXP}$, colored dots) versus unexpanded ($CD8_{UNEXP}$, gray dots) $CD8^+$ clonotypes from the participant at PTD 111 (left plot) and PTD 125 (right plot). $CD8_{EXP}$ first expanded on PTD 111 are shown in pink and those first expanding on PTD 125 are shown in blue. **(E)** Heatmap shows average expression of unsupervised differentially expressed genes found between $CD8_{EXP}$ at each timepoint.

Figure 7. Temporal scRNAseq analysis of the response to anti-rejection therapy under iscalimab maintenance immunosuppression (IS). A participant on iscalimab

IS (ISCAL_1) was diagnosed with ACR 1A on post-transplant day (PTD) 60 and a biopsy was obtained prior to anti-rejection treatment with tacrolimus. A second biopsy was obtained on PTD 78 and the participant was diagnosed with no rejection. A third biopsy was taken at PTD 336 and the participant was again diagnosed with no rejection. **(A)** Pie charts display number and frequency of expanded clonotypes found in the index biopsy (PTD 60) and subsequent follow-up biopsies (PTD 78, PTD 336). Bar graph shows overlapping clonotypes across the 3 timepoints. **(B)** UMAP shows $CD8^+$ clusters in an integrated analysis of all timepoints. **(C)** Violin plots show relative expression level of indicated genes selected to characterize cell cluster phenotypes as activated, exhausted, and memory. **(D)** Temporal analysis of $CD8_{EXP}$ following anti-rejection therapy. UMAP plots show clustering of expanded ($CD8_{EXP}$, colored dots) versus unexpanded ($CD8_{UNEXP}$, gray dots) $CD8^+$ clonotypes from the participant at PTD 60 (left plot); PTD 78 (middle plot); or PTD 336 (right plot). $CD8_{EXP}$ emerging on PTD 60 are shown in pink, those emerging on PTD 78 are shown in green, and those emerging on PTD 336 are shown in blue. **(E)** Heatmap shows average expression of unsupervised differentially expressed genes ($p<0.05$) found between $CD8_{EXP}$ at each timepoint.

Figure 8. Comparison of $CD8_{EXP}$ between the biopsy and paired urine samples in a participant undergoing treatment-refractory rejection. A participant on iscalimab immunosuppression (ISCAL_3) was diagnosed with ACR 1B on post-transplant day (PTD) 137 and a biopsy was obtained prior to anti-rejection treatment with tacrolimus conversion and steroids. A second biopsy was obtained on PTD 151 and the participant was diagnosed with ACR 1B. MMF was then added to the anti-rejection regimen. A third

biopsy was taken at PTD 179 and the participant was diagnosed as borderline and MMF was tapered off. A final biopsy was taken at PTD 291 and showed mixed 1B rejection. **(A, B)** Pie charts (top) display number and frequency of expanded clonotypes found at each biopsy **(A)** and urine **(B)** sample and bar graphs (bottom) display clonotypes found at the indicated timepoint. Different colors represent individual expanded clonotypes (gray area represents unexpanded clonotypes) and the size of the colored area represents the relative size of the expanded clonotypes. **(C)** Venn diagrams display overlap of individual $CD8_{EXP}$ clonotypes between biopsies and their paired urine sample at the indicated timepoints.

Figure 9. Temporal scRNAseq analysis of treatment-refractory rejection under iscalimab maintenance immunosuppression (IS). (A) Allograft-derived $CD8^+$ T cells from all timepoints from participant ISCAL_3 were integrated and renormalized and UMAP plot shows individual $CD8^+$ clusters based on differentially expressed genes. Note that some clusters are unique to individual timepoints. **(B)** Violin plots show relative expression level of indicated genes selected to characterize cell cluster phenotypes as activated, exhausted, and memory. **(C)** Temporal analysis of $CD8_{EXP}$ during treatment-refractory rejection therapy. UMAP plots show clustering of expanded ($CD8_{EXP}$, colored dots) versus unexpanded ($CD8_{UNEXP}$, gray dots) $CD8^+$ clonotypes from the participant at PTD 137 (left plot); PTD 151 (middle left plot); PTD 179 (middle right plot); or PTD 291 (right plot). $CD8_{EXP}$ emerging on PTD 137 are shown in pink, on PTD 151 are shown in green, PTD 179 are shown in blue, and those emerging on PTD 291

766 are shown in purple. **(D)** Heatmap shows average expression of unsupervised
767 differentially expressed genes found between expanded clonotypes at each timepoint.
768
769
770
771
772
773
774
775
776
777
778
779
780
781
782
783
784
785
786
787

References

1. Wojciechowski D, Wiseman A. Long-Term Immunosuppression Management: Opportunities and Uncertainties. Clin J Am Soc Nephrol. 2021;16(8):1264-1271.

2. Randhawa PS, et al. The Histopathological Changes Associated with Allograft Rejection and Drug Toxicity in Renal Transplant Recipients Maintained on FK506. Am J Surg Pathol. 1993;17(1):60-8.

3. Vincenti F, et al. Belatacept and Long-Term Outcomes in Kidney Transplantation. New Engl J Med. 2016;374(4):333-43.

4. Woodle ES, et al. Belatacept-based immunosuppression with simultaneous calcineurin inhibitor avoidance and early corticosteroid withdrawal: A prospective, randomized multicenter trial. Am J Transplant. 2020;20(4):1039-55.

5. Castro Rojas, CM, et al. mTOR Inhibitor Therapy Diminishes Circulating CD8+ CD28- Effector Memory T Cells and Improves Allograft Inflammation in Belatacept-refractory Renal Allograft Rejection. Transplantation. 2020;104(5)1058-1069.

6. Vincenti F, et al. A phase III study of belatacept-based immunosuppression regimens versus cyclosporine in renal transplant recipients (BENEFIT study). Am J Transplant. 2010;10(3):535-46.

7. Ristov J, et al. Characterization of the in vitro and in vivo properties of CFZ533, a blocking and non-depleting anti-CD40 monoclonal antibody. Am J Transplant. 2018;18(12):2895-904.

8. Ulrich P, et al. Nonclinical Safety Assessment of CFZ533, a Fc-Silent Anti-CD40 Antibody, in Cynomolgus Monkeys. Toxicol Sci. 2018;166(1):192-202.

9. Cordoba F, et al. A novel, blocking, Fc-silent anti-CD40 monoclonal antibody prolongs nonhuman primate renal allograft survival in the absence of B cell depletion. Am J Transplant. 2015;15(11):2825-36.

10. Mohiuddin MM, et al. Role of anti-CD40 antibody-mediated costimulation blockade on non-Gal antibody production and heterotopic cardiac xenograft survival in a GTKO.hCD46Tg pig-to-baboon model. Xenotransplantation. 2014;21(1):35-45.

11. Higginbotham L, et al. Pre-transplant antibody screening and anti-CD154 costimulation blockade promote long-term xenograft survival in a pig-to-primate kidney transplant model. Xenotransplantation. 2015;22(3):221-30.

12. Mohiuddin MM, et al. Chimeric 2C10R4 anti-CD40 antibody therapy is critical for long-term survival of GTKO.hCD46.hTBM pig-to-primate cardiac xenograft. Nat Commun. 2016;7(1):11138.

13. Vincenti F, et al. A randomized, phase 1b study of the pharmacokinetics, pharmacodynamics, safety, and tolerability of bleselumab, a fully human, anti-CD40 monoclonal antibody, in kidney transplantation. Am J Transplant. 2020;20(1):172-80.

14. Harland RC, et al. Efficacy and safety of bleselumab in kidney transplant recipients: A phase 2, randomized, open-label, noninferiority study. Am J Transplant. 2020;20(1):159-71.

15. Rocha PN, et al. Effector mechanisms in transplant rejection. Immunol Rev. 2003;196:51-64.

16. Morris H, et al. Tracking donor-reactive T cells: Evidence for clonal deletion in tolerant kidney transplant patients. Sci Transl Med. 2015;7(272):272ra10 .

17. Dewolf S, et al. Quantifying size and diversity of the human T cell alloresponse. JCI Insight. 2018;3(15):e121256.

18. Zeng G, et al. Antigen-Specificity of T Cell Infiltrates in Biopsies With T Cell–Mediated Rejection and BK Polyomavirus Viremia: Analysis by Next Generation Sequencing. Am J Transplant. 2016;16(11):3131-8.

19. Lai L, et al. T cell repertoire following kidney transplantation revealed by high-throughput sequencing. Transpl Immunol. 2016;39:34-35.

20. Alachkar H, et al. Quantitative characterization of T-cell repertoire and biomarkers in kidney transplant rejection. BMC Nephrol. 2016;17(1):181.

21. Famulski KS, et al. Defining the Canonical Form of T-Cell-Mediated Rejection in Human Kidney Transplants. Am J Transplant. 2010;10(4):810-20.

22. Reeve J, et al. Molecular Diagnosis of T Cell-Mediated Rejection in Human Kidney Transplant Biopsies. Am J Transplant. 2013;13(3):645-55.

23. Halloran PF, et al. Molecular phenotype of kidney transplant indication biopsies with inflammation in scarred areas. Am J Transplant. 2019;19(5):1356-1370.

24. Tang F, et al. mRNA-Seq whole-transcriptome analysis of a single cell. Nat Methods. 2009;6(5):377-82.

25. Han A, et al. Linking T-cell receptor sequence to functional phenotype at the single-cell level. Nat Biotechnol. 2014;32(7):684-92.

26. Wu H, et al. Single-Cell Transcriptomics of a Human Kidney Allograft Biopsy Specimen Defines a Diverse Inflammatory Response. J Am Soc Nephrol. 2018;29(8):2069-2080.

27. Malone AF, et al. Harnessing Expressed Single Nucleotide Variation and Single Cell RNA Sequencing To Define Immune Cell Chimerism in the Rejecting Kidney Transplant. J Am Soc Nephrol. 2020;31(9):1977-1986.

28. Snyder ME, et al. Modulation of tissue resident memory T cells by glucocorticoids after acute cellular rejection in lung transplantation. J Exp Med. 2022;219(4):e20212059.

29. Arazi A, et al. The immune cell landscape in kidneys of patients with lupus nephritis. Nat Immunol. 2019;20(7):902-14.

30. Donlin LT, et al. Methods for high-dimensional analysis of cells dissociated from cryopreserved synovial tissue. Arthritis Res Ther. 2018;20(1):139.

31. Adam M, et al. Psychrophilic proteases dramatically reduce single cell RNA-seq artifacts: A molecular atlas of kidney development. Development. 2017;144(19):3625-32.

32. Stewart BJ, et al. Spatiotemporal immune zonation of the human kidney. Science. 2019;365(6460):1461-6.

33. Crowe S, et al. Quantitative immunocytofluorographic analysis of CD4 surface antigen expression and HIV infection of human peripheral blood monocyte/macrophages. AIDS Res Hum Retrov. 1987;3(2):135-45.

945 34. Behr FM, et al. Circulating memory CD8+ T cells are limited in forming CD103+
946 tissue-resident memory T cells at mucosal sites after reinfection. Eur J Immunol.
947 2021;51(1):151-66.
948 35. Kok L, et al. The precursors of CD8+ tissue resident memory T cells: from lymphoid
949 organs to infected tissues. Nat Rev Immunol. 2022;22(5):283-93.
950 36. Mackay LK, et al. Hobit and Blimp1 instruct a universal transcriptional program of
951 tissue residency in lymphocytes. Science. 2016;352(6284):459-63.
952 37. Crowl JT, et al. Tissue-resident memory CD8+ T cells possess unique
953 transcriptional, epigenetic and functional adaptations to different tissue environments. Nat
954 Immunol. 2022;23(7):1121-31.
955 38. de Leur K, et al. Characterization of donor and recipient CD8+ tissue-resident
956 memory T cells in transplant nephrectomies. Sci Rep. 2019;9(1):5984.
957 39. Khan O, et al. TOX transcriptionally and epigenetically programs CD8+ T cell
958 exhaustion. Nature. 2019;571(7764):211-8.
959 40. Heemskerk MH, et al. Redirection of antileukemic reactivity of peripheral T
960 lymphocytes using gene transfer of minor histocompatibility antigen HA-2-specific T-cell
961 receptor complexes expressing a conserved alpha joining region. Blood.
962 2003;102(10):3530-40.
963 41. Mathews DV, et al. Belatacept-Resistant Rejection Is Associated With CD28+
964 Memory CD8 T Cells. Am J Transplant. 2017;17(9):2285-2299.
965 42. Aschauer C, et al. Prospective Tracking of Donor-Reactive T-Cell Clones in the
966 Circulation and Rejecting Human Kidney Allografts. Front Immunol. 2021;12:750005.

43. Brehm MA, et al. Allografts stimulate cross-reactive virus-specific memory CD8 T cells with private specificity. Am J Transplant. 2010;10(8):1738-48.

44. van den Heuvel H, et al. Infection with a virus generates a polyclonal immune response with broad alloreactive potential. Hum Immunol. 2019;80(2):97-102.

45. Snyder ME, Finlayson MO, Connors TJ, Dogra P, Senda T, Bush E, et al. Generation and persistence of human tissue-resident memory T cells in lung transplantation. Sci Immunol. 2019;4(33):eaav5581.

46. Yuan R, et al. Critical role for CD103+CD8+ effectors in promoting tubular injury following allogeneic renal transplantation. J Immunol. 2005;175(5):2868-79.

47. Kaminski H, et al. Characterization of a unique γδ T-cell subset as a specific marker of cytomegalovirus infection serverity. J Infect Dis 2021;224(4):655-666.

48. Couzi L, et al. Direct and indirect effects of cytomegalovirus-induced γδ T cells after kidney transplantation. Front Immunol 2015;21(6):3.

49. Satija R, et al. Spatial reconstruction of single-cell gene expression data. Nat Biotechnol. 2015;33(5):495-502.

50. Stuart T, et al. Comprehensive integration of single-cell data. Cell. 2019;177(7):1888-902.e21.

51. Nazarov V, et al. immunarch: bioinformatics analysis of T-cell and B-cell immune repertoires. https://githubcom/immunomind/immunarch. 2022.

52. Kowarz E, et al. Optimized Sleeping Beauty transposons rapidly generate stable transgenic cell lines. Biotechnol J. 2015;10(4):647-53.

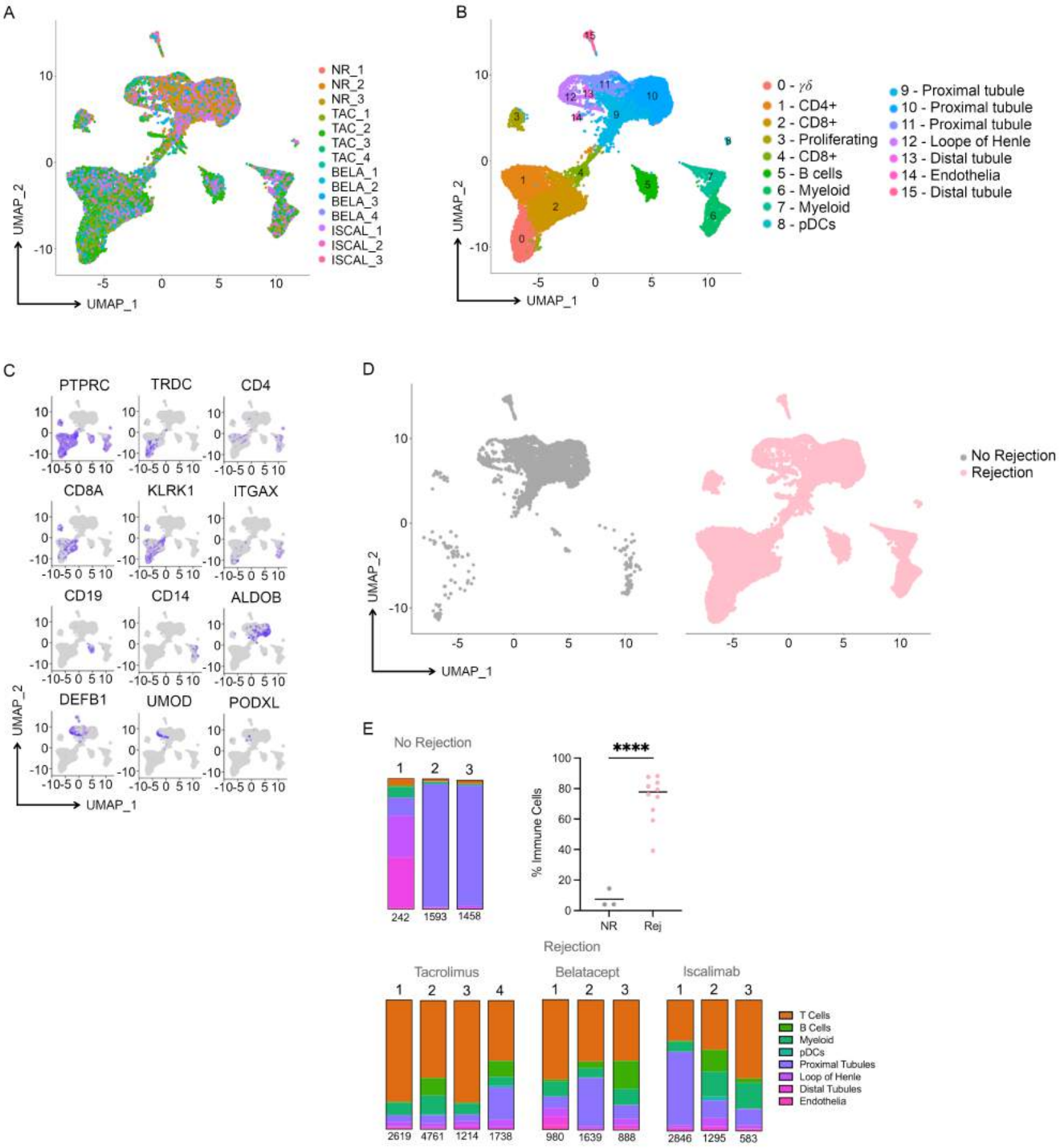

Figure 1. Single cell RNA sequencing analysis of transplanted kidney allografts. Single cell suspensions from thirteen different biopsies (3 without rejection, 10 with rejection) were individually subjected to 5' single cell RNAseq on the 10X platform with V(D)J sequencing. After alignment using Cell Ranger, cells with >25% mitochondrial content and <200 genes, including additional low-quality cells, were removed, and samples were integrated using Seurat. (A, B) UMAP plots display cell contribution by sample and cell type. (C) Expression of "signature" genes across cell types. Blue color intensity reflects the expression level of individual genes within given cells. (D) Separation of samples based on rejection status. UMAP plots show cells from no rejection samples (gray, left plot) versus rejection samples (pink, right plot). (E) Frequency of cell types within each sample are displayed in bar graphs. Statistical analyses reveal a significantly increased proportion of immune infiltration in the rejection samples (n=10) as compared to the no rejection samples (n=3) [two-tailed t-test, ****p<0.0001].

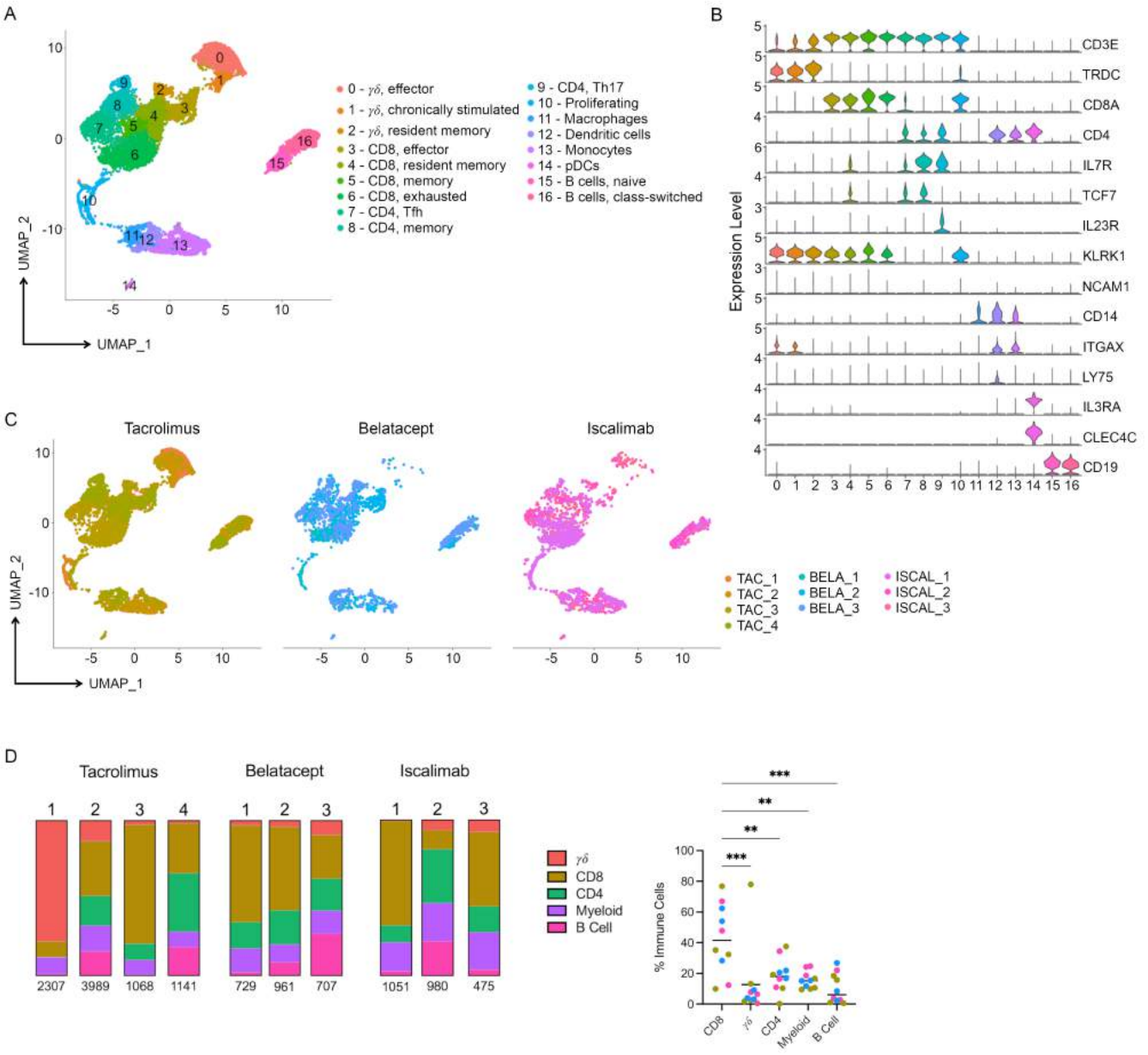

Figure 2. Diverse immune cell infiltrate during kidney allograft rejection. Index samples from the 10 participants undergoing rejection were integrated, clusters annotated as non-immune cells were remove, and the data were re-normalized and re-clustered using Seurat. (A) UMAP plot shows immune cell clusters and accompanying annotations. (B) Violin plots display the relative gene expression level of indicated genes across each cluster. (C) Samples were segrated according to maintenance IS type. UMAP plots show immune cell clustering of samples from participants with rejection under tacrolimus (left plot, shades of mustard); belatacept (middle plot, shades of blue); or iscalimab (right plot, shades of pink) maintenance immunosuppression. (D) Frequency of cell types within each sample are displayed in bar graphs. Statistical analyses reveal a significantly increased proportion of CD8+ T cells in the immune infiltration as compared to other immune subtypes (n=10) [one-way ANOVA, ***p<0.0006, **p<0.007].

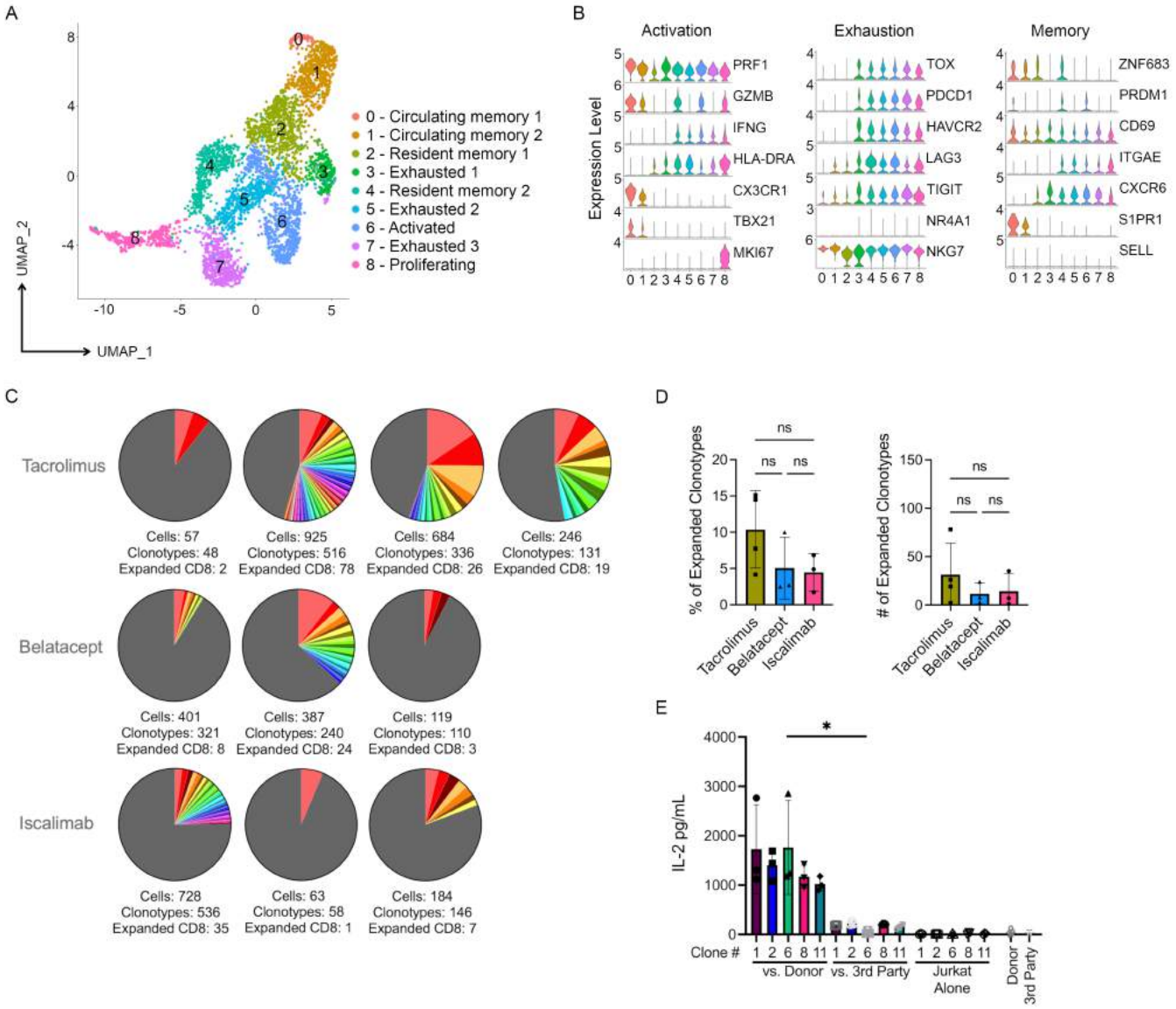

Figure 3. Analysis of infiltrating CD8+ T cells in kidney allograft rejection. CD8+ clusters from the immune cell analysis were identified for futher analyses; CD4+ and γδ T cells were removed. The samples were then re-analyzed using Seurat. (A) UMAP plot shows cell type annotations based on differentially expressed genes. (B) Violin plots show relative expression level of indicated genes selected to characterize cell cluster phenotypes as activated, exhausted, and memory. (C) Pie charts display nunmber and frequency of expanded CD8+ clonotypes (CD8EXP) found in the biopsy during rejection by participant sample, based on their unique CDR3αβ sequences. Expanded clonotypes are defined as having >2 cells with identical CDR3αβ sequences. Different colors represent individual expanded clonotypes (gray area represents unexpanded clonotypes) and the size of the colored area represents the relative size of the expanded clonotypes. (D) The percentage (left graph) and total number (right graph) of CD8EXP in each treatment group (tacrolimus n=4, belatacept n=3, iscalimab n=3) are displayed in bar braphs (+/- SD) [one-way ANOVA, ns = not significant, p> 0.05]. (E) Full length TCRs with unique CDR3αβ sequences derived from 5 CD8EXP from one participant experiencing rejection (ISCAL_1) were subcloned into individual Jurkat76 cells. Individual clones were cultured in triplicate either alone, with donor, or with 3rd party T cell-depleted PBMCs for 20 hours and IL-2 levels in the supernatant were measured via ELISA. Results show the lvels of IL-2 in pg/mL for each condition (+/- SD) done in triplicates (n=3) [one-way ANOVA, *p<0.05].

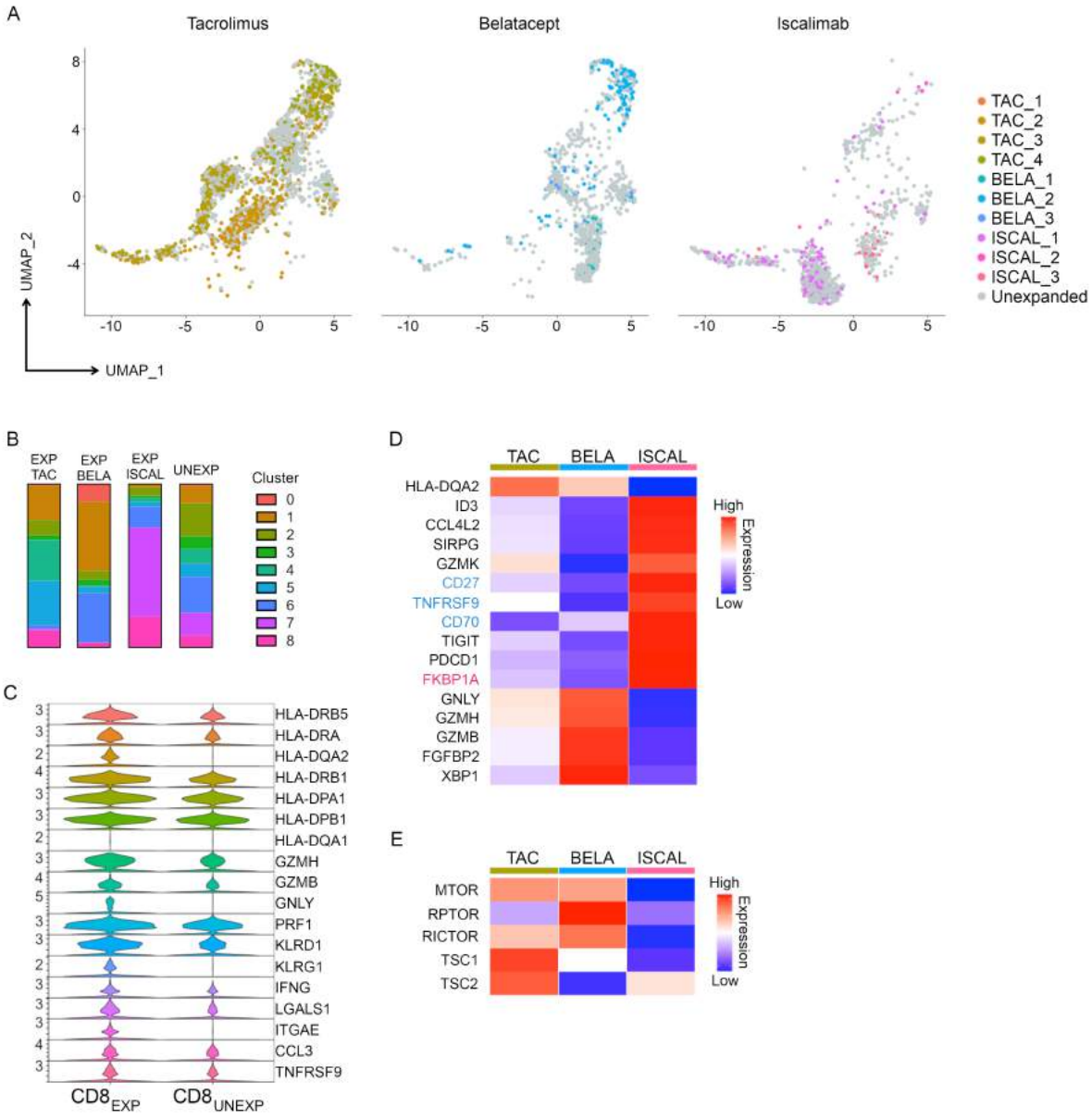

Figure 4. Gene expression differences in CD8EXP between tacrolimus, belatacept, and iscalimab maintenance IS. (A) Clustering of CD8EXP based on maintenance IS type. UMAP plots show clustering of CD8EXP (colored dots) versus CD8UNEXP (gray dots) from participants under either tacrolimus (left plot, shades of mustard); belatacept (middle plot, shades of blue); or iscalimab (right plot, shades of pink) maintenance IS. (B) Bar graphs display the fraction of expanded clonotypes (tacrolimus, belatacept, or iscalimab) and unexpanded clonotypes contributing to each CD8+ T cell cluster. (C) Violin plots show the relative expression of indicated genes in expanded (CD8EXP) and unexpanded (CD8UNEXP) CD8+ clonotypes. (D) Heatmap displays (average) expression of unsupervised differentially expressed genes ($p<0.05$) in CD8EXP under tacrolimus (n=4), belatacept n=3), and iscalimab (n=3) maintenance IS. Blue text denotes 3 TNF family member genes and red text denotes *FKBP1A*, a target of tacrolimus. (E) Heatmap displays a supervised analysis of the average expression of mTOR pathway-related genes in CD8EXP from participants under tacrolimus, belatacept, and iscalimab maintenance IS.

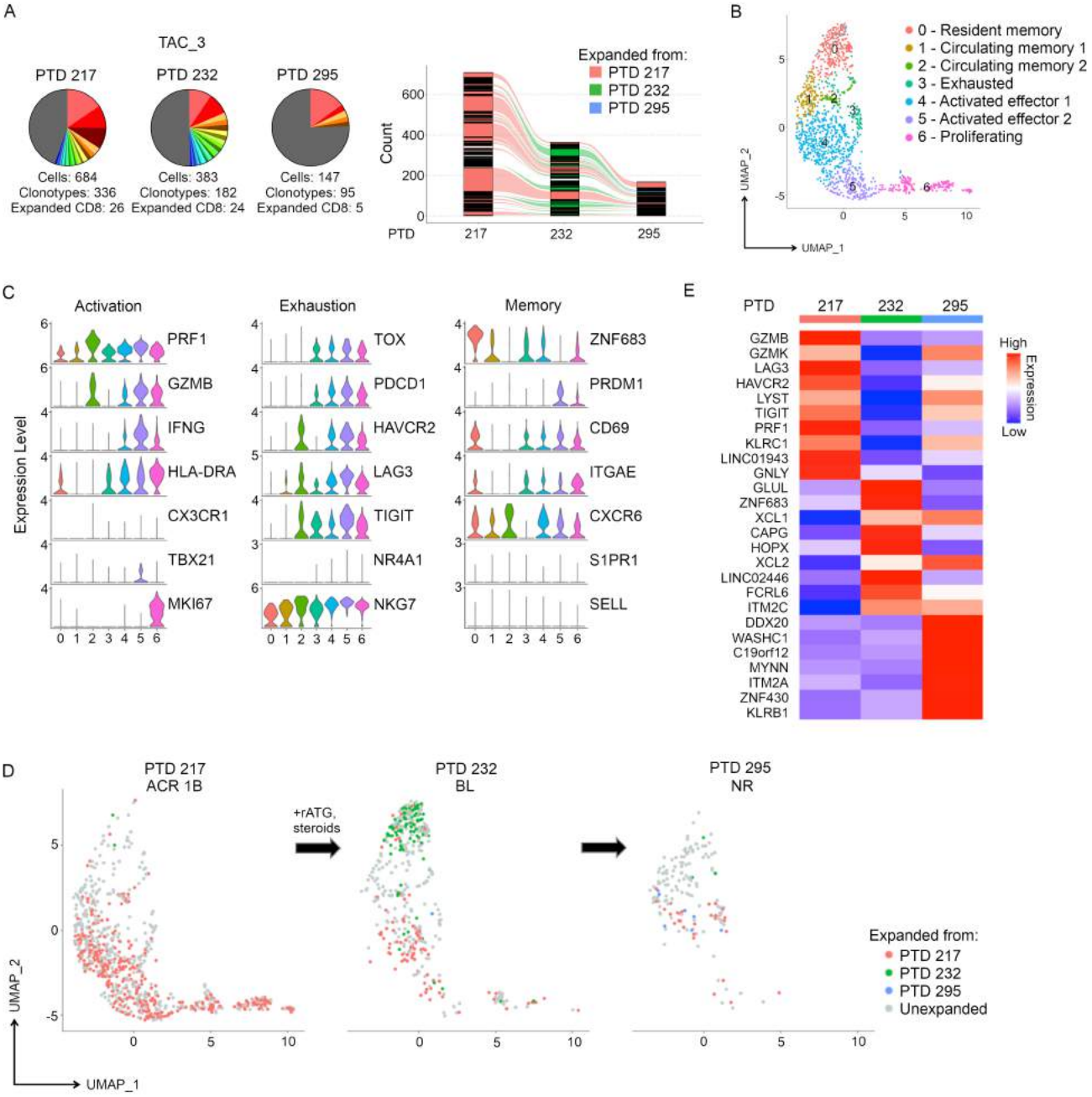

Figure 5. Temporal scRNAseq analysis of the response to anti-rejection therapy under tacrolimus maintenance immunosuppression (IS). A participant on tacrolimus IS (TAC_3) was diagnosed with ACR 1B on post-transplant day (PTD) 217 and a biopsy was obtained prior to anti-rejection treatment with rATG and steroids. A second biopsy was obtained on PTD 232 and the participant was diagnosed with a borderline lesion. A third biopsy was taken at PTD 295 and the participant was diagnozed with no rejection. (A) Pie charts display number and frequency of expanded clonotypes found in the index biopsy (PTD 217) and subsequent follow-up biopsies (PTD 232, PTD 295). Bar graph shows overlapping clonotypes across 3 timepoints. (B) UMAP shows CD8+ clusters in an integrated analysis of all timepoints. (C) Violin plots show relative expression level of indicated genes selected to characterize cell cluster phenotypes as activated, exhausted, and memory. (D) Temporal analysis of $CD8^{EXP}$ following anti-rejection therapy. UMAP plots show clustering of expanded ($CD8^{EXP}$, colored dots) versus unexpanded ($CD8^{UNEXP}$, gray dots) CD8+ clonotypes from the participant at PTD 217 (left plot); PTD 232 (middle plot); or PTD 295 (right plot). $CD8^{EXP}$ first expanded on PTD 217 are shown in pink, those first expanding on PTD 232 are shown in green, and those first expanding on PTD 295 are shown in blue. (E) Heatmap shows average expression of unsupervised differentially expressed genes ($p<0.05$) found between $CD8^{EXP}$ at each timepoint.

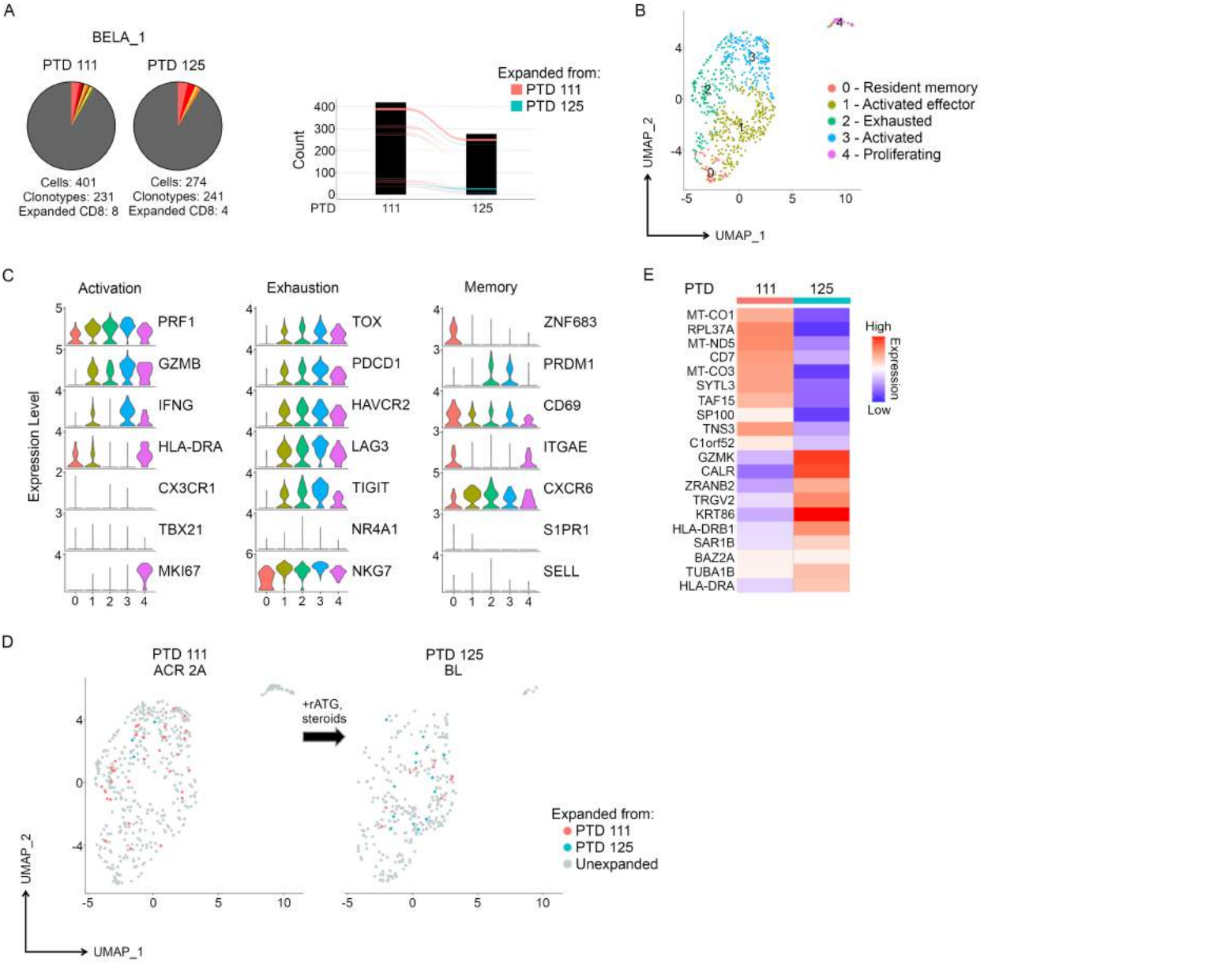

Figure 6. Temporal scRNAseq analysis of the response to anti-rejection therapy under belatacept maintenance immunosuppression (IS). A participant on belatacept IS (BELA_1) was diagnosed with ACR 2A on post-transplant day (PTD) 111 and a biopsy was obtained prior to anti-rejection treatment with rATG and steroids. A second biopsy was obtained on PTD 125 and the participant was diagnosed with a borderline lesion. (A) Pie charts display number and frequency of expanded clonotypes found in the index biopsy (PTD 111) and the subsequent follow-up biopsy (PTD 125). Bar graph shows overlapping clonotypes across the two individual timepoints. (C) Violin plots show relative expression level of indicated genes selected to characterize cell cluster phenotypes as activated, exhausted, and memory. (D) Temporal analysis of CD8EXP following anti-rejection therapy. UMAP plots show clustering of expanded (CD8EXP, colored dots) versus unexpanded (CD8UNEXP, gray dots) CD8+ clonotypes from the participant at PTD 111 (left plot) and PTD 125 (right plot). CD8EXP first expanded on PTD 111 are shown in pink and those first expanding on PTD 125 are shown in blue. (E) Heatmap shows average expression of unsupervised differentially expressed genes found between CD8EXP at eatch timepoint.

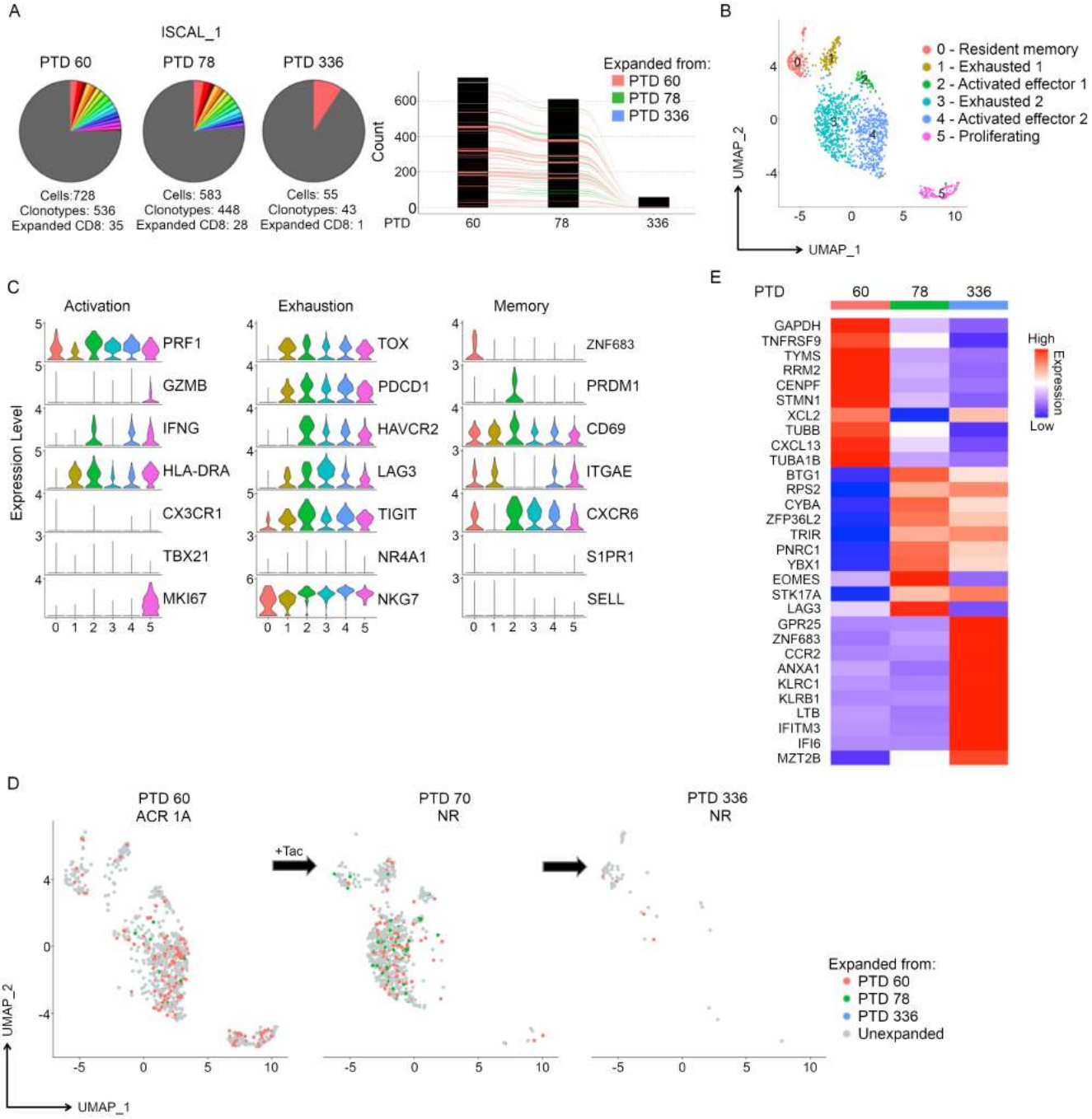

Figure 7. Temporal scRNAseq analysis of the response to anti-rejection therapy under iscalimab maintenance immunosuppression (IS). A participant on iscalimab IS (ISCAL_1) was diagnosed with ACR 1A on post-transplant day (PTD) 60 and a biopsy was obtained prior to anti-rejection treatment with tacrolimus. A second biopsy was obtained on PTD 78 and the participant was diagnosed with no rejection. A third biopsy was taken at PTD 336 and the participant was again diagnosed with no rejection. (A) Pie charts display the number and frequency of expanded clonotypes found in the index biopsy (PTD 60) and subsequent follow-up biopsies (PTD 78, PTD 336). Bar graph shows overlapping clonotypes across the 3 timepoints. (B) UMAP shows CD8+ clusters in an integrated analysis of all timepoints. (C) Violin plots show relative expression level of indicated genes selected to characterize cell cluster phenotypes as activated, exhausted, and memory. Temporal analysis of $CD8^{EXP}$ following anti-rejection therapy. UMAP plots show clustering of expanded ($CD8^{EXP}$, colored dots) versus unexpanded ($CD8^{UNEXP}$, gray dots) from the participant at PTD 60 (left plot); PTD 78 (middle plot); or PTD 336 (right plot). $CD8^{EXP}$ emerging on PTD 60 are shown in pink, those emerging on PTD 78 are shown in green, and those emerging on PTD 336 are shown in blue. (E) Heatmap shows average expression of unsupervised differentially expressed genes ($p<0.05$) found between $CD8^{EXP}$ at each timepoint.

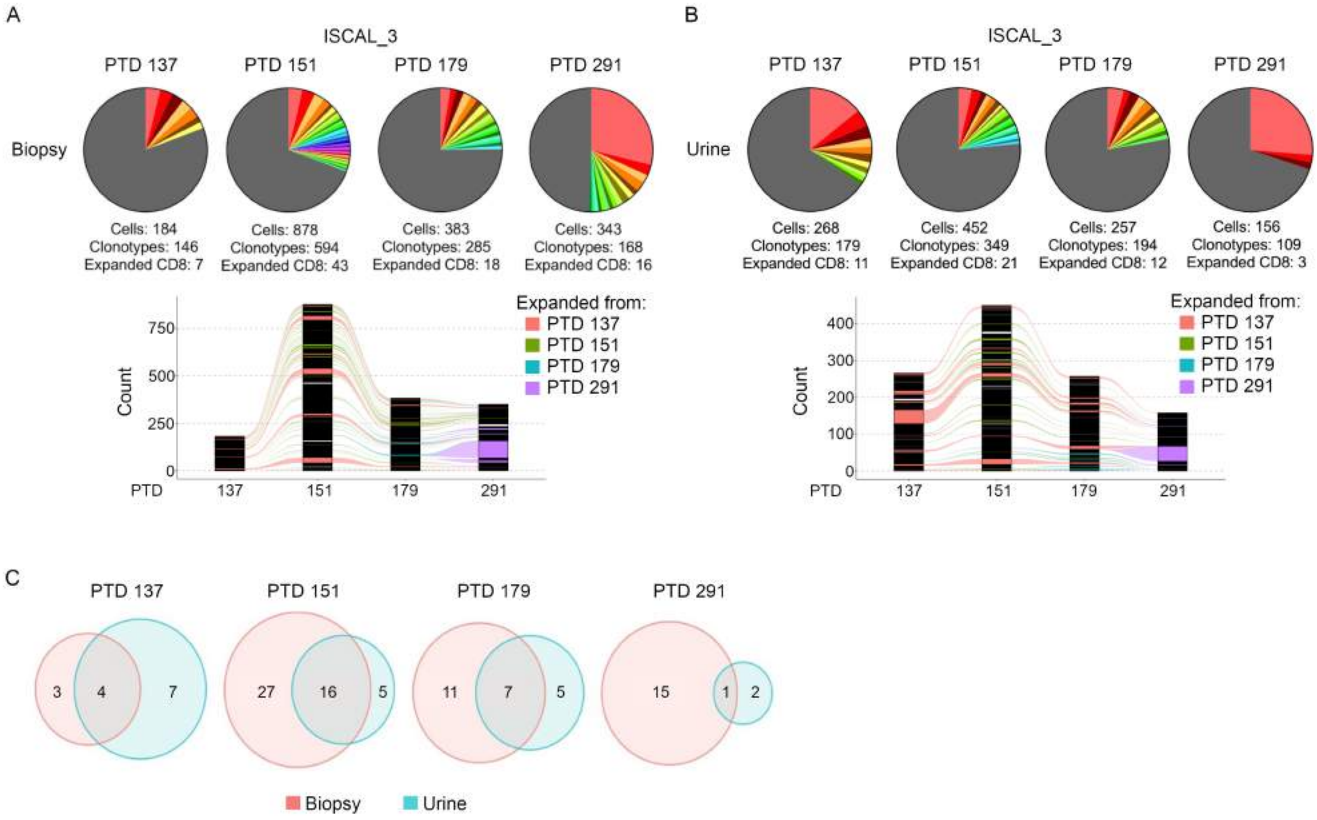

Figure 8. Comparison of CD8EXP between the biopsy and paired urine samples in a participant undergoing treatment-refractory rejection. A participant on iscalimab maintenance immunosuppression (ISCAL_3) was diagnosed with ACR 1B on post-transplant day (PTD 137) and a biopsy was obtained prior to anti-rejection therapy with tacrolimus conversion and steroids. A second biopsy was obtained on PTD 151 and the participant was diagnosed with ACR 1B. MMF was then added to the anti-rejection regimen. A third biopsy was taken at PTD 179 and the participant was diagnosed as borderline and MMF was tapered off. A final biopsy was taken at PTD 291 and showed mixed 1B rejection. (A, B). Pie charts (top) display number and frequency of expanded clonotypes found at each biopsy (A) and urine (B) sample and bar graphs (bottom) display clonotypes found at the indicated timepoint. Different colors represent individual expanded clonotypes (gray area represents unexpanded clonotypes) and the size of the colored area represents the relative size of the expanded clonotypes. (C) Venn diagrams display overlap of individual CD8EXP clonotypes between biopsies and their paired urine sample at the indicated timepoints.

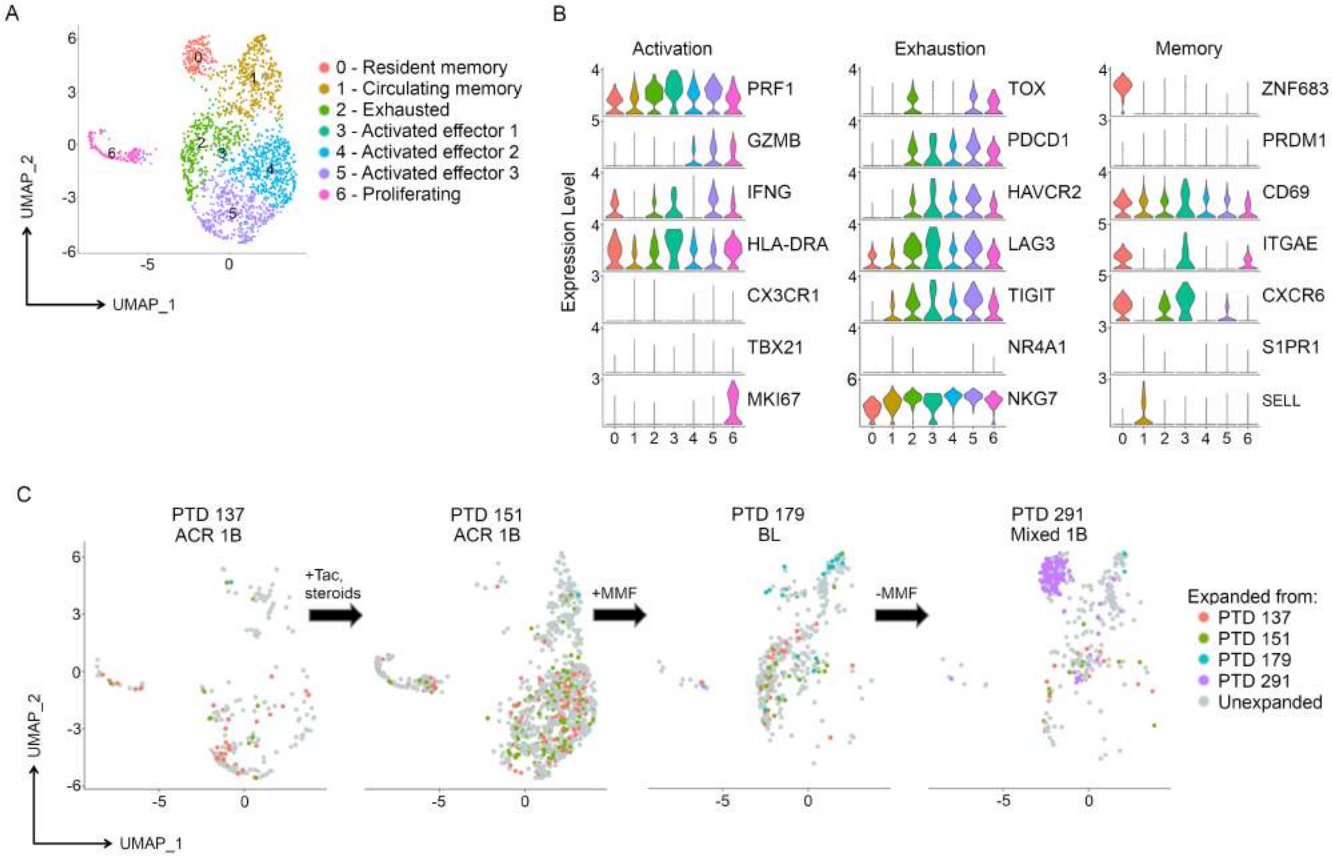

Figure 9. Temporal scRNAseq analysis of treatment-refractory rejection under iscalimab maintenace immunosuppression (IS). (A) Allograft-derived CD8+ T cells from all timepoints from participant ISCAL_3 were integrated and renormalized and UMAP plot shows individual CD8+ clusters based on differentially expressed genes. Note that some clusters are unique to individual timepoints. (B) Violin plots show relative expression level of indicated genes selected to characterize cell cluster phenotypes as activated, exhausted, and memory. (C) Temporal analysis of CD8EXP during treatment-refractory rejection. UMAP plots show clustering of expanded (CD8EXP, colored dots) versus unexpanded (CD8UNEXP, gray dots) CD8+ clonotypes from the participant at PTD 137 (left plot); PTD 151 (middle left plot); PTS 179 (middle right plot); or PTD 291 (right plot). CD8EXP emerging on PTS 137 are shown in pink, on PTD 151 are shown in green, PTD 179 are shown in blue, and those emerging on PTD 291 are shown in purple. (D) Heatmap shows average expression of unsupervised differentially expressed genes found between expanded clonotypes at each timepoint.

Table 1. Participant demographics of the 13 samples included in the index biopsy analyses.

Rej. Group	Patient ID	Age	Sex	Race	Etiology of ESRD*	Txp No.	Donor Type+	No. HLA Mismatches#		MIS at Time of Biopsy$
								Class I	Class II	
Non-Rejection Cohort	NR_1	23	M	C	Alport	1	LD	6	3	Tac/MMF
	NR_4	65	M	C	DM1	1	LD	5	5	Iscal/MMF/Pred
	NR_5	62	M	C	TBMD	1	LD	3	5	Iscal/MMF/Pred
Rejection under Tacrolimus	TAC_1	54	F	C	DM1	2	DD	1	1	Tac/MMF
	TAC_2	62	F	C	DM1	1	DD	3	5	Tac/MMF/Pred
	TAC_3	21	M	C	PKD	2	DD	4	4	Tac/MMF/Pred
	TAC_4	35	F	C	ObsUro	1	DD	5	3	Tac/MMF
Rejection under Belatacept	BELA_1	68	M	C	DM2	1	LD	3	3	Bela/MMF
	BELA_2	31	F	C	FSGS	1	LD	5	5	Bela/MMF
	BELA_3	34	M	AA	aHUS	1	DD	5	5	Bela/MMF
Rejection under Iscalimab	ISCAL_1	55	F	AA	GSG	1	LD	2	1	Iscal/MMF/Pred
	ISCAL_2	23	M	C	conVUR	1	LD	5	3	Iscal/MMF/Pred
	ISCAL_3	41	F	AA	FSGS	1	DD	6	5	Iscal/Pred

Notes:

*ESRD, end-stage renal disease; PKD, polycystic kidney disease; HTN, hypertension; DM1, diabetes mellitus type 1; TBMD, thin basement membrane disease; FSGS, focal segmental glomerulosclerosis; conVUR, congenital vesicoureteral reflux; GSG, globally sclerotic glomeruli; ObsUro, obstructive uropathy; DM2, diabetes mellitus type 2; aHUS, atypical hemolytic uremic syndrome

+ LD, living donor; DD, deceased donor

Alleles included were MHC-Class I: HLA-A, -B, -C, and β-chains of MHC-Class II: DRB, DQB, DPB (12 alleles total)

$ IS, immunosuppression; Tac, tacrolimus; MMF, mycophenolate mofetil; Iscal, iscalimab; Pred, prednisone; Bela, belatacept; all patients received the standard induction IS of anti-rabbit thymoglobulin, MMF and Pred (with taper)

Individual participant information for temporal scRNAseq analysis of the response to anti-rejection therapy.

Patient ID	IS at Time of Biopsy	Anti-Rejection Therapy Prior to Biopsy	PTD	Rej Type	ACR Rej Grade	Pathology Composite Score													DSA Status
						v	t	i	g	ptc	ci	ct	cg	cv	mm	ah	ti	c4d	
TAC_3	Tac/MMF/Pred	.	217	ACR	1B	0	3	3	1	1	0	0	0	0	0	0	3	1+	Neg
		rATG; Pred	232	ACR	BL	0	1	1	1	1	1	1	0	0	0	0	1	0	Neg
		None	295	NR	0	0	1	0	0	1	2	2	0	0	0	1	1	1	Neg
BELA_1	Bela/MMF	Pred	111	ACR	2A	1	1	1	0	1	1	1	0	0	1	1	.	0	Neg
		rATG; Pred	125	ACR	BL	1	1	1	0	1	1	1	0	2	1	1	.	+	Neg
ISCAL_1	Iscal/MMF/Pred	rATG; Pred	60	ACR	1A	0	2	1	0	0	0	0	0	0	0	0	.	+	Neg
		Tac Added	78	NR	0	0	1	0	0	0	0	0	0	0	0	0	.	+	Neg
		Tac Tapered Off	336	NR	0	0	1	0	0	0	0	0	0	2	0	0	0	0	Unk
ISCAL_3	Iscal/Pred	.	137	ACR	1B	0	3	3	0	1	1	1	0	0	0	0	3	1+	Neg
		Tac Conversion; Pred	151	ACR	1B	0	3	2	1	0	1	1	0	0	.	0	.	1	Neg
		MMF Added	179	ACR	BL	0	3	1	1	0	3	3	0	2	.	0	.	2	Neg
		MMF Held	291	Mixed	1B	0	3	2	1	2	2	2	0	3	.	0	.	3	Pos